THE UNIVERSITY OF BIRMINGHAM

NANOSCALE MAGNESIUM AS A HYDROGEN STORAGE MATERIAL

By: Athanasia Paloumpi

Supervisor: Dr. David Book

A thesis submitted to the Department of Metallurgy and Materials for the degree of Master of Research

Department of Metallurgy and Materials
The University of Birmingham
June 2010

Contents

Acknowledgments

This section is dedicated to expressing my gratitude to all the people who assisted me throughout my research. First of all, I would like to thank my supervisor Dr. David Book who was always willing to provide his well-aimed advice and insight on many aspects of this work. His guidance and expertise were more than valuable to this work and a great source of personal knowledge.

Many thanks go to Teer Coatings Ltd and especially to Joanne Hampshire for providing valuable help at a very difficult time during my project by supplying us with thin film samples. I would also like to thank Dr. Isaac Chang (Dept. of Metallurgy and Materials) and Metal Nanopowders Ltd. for providing us with Mg nanopowder samples used in this work.

My greatest gratitude goes to Dan, Vicky and Allan as well as the rest of the 'Hydrogen Team' who patiently guided and supported me throughout this year. Finally, my special thanks go to my colleagues and close friends Jun, Pierre and Alessandro whose enjoyable presence makes me yearn for even the most difficult days in the lab.

Abstract

This work investigates the structural and hydrogenation properties of nanoscale magnesium in various forms (powders of various mesh sizes as well as thin films) which have been proven to overcome the major drawbacks of Mg as a mean of solid state hydrogen storage. In this study we also propose a structure consisting of a Mg and Ti multilayered thin films. The hydrogen storage performance and the structures of these Mg/Ti thin film multilayer samples (which were successfully deposited upon various substrates using a magnetron sputtering system) are also investigated in this study.

SEM and XRD allowed us to observe the structures and composition of the Mg and Mg/Ti thin film samples. XRD confirmed a (002) preferential orientation of the films in agreement with literature. Differences in the sputtering conditions of the Mg/Ti samples also gave rise to differences in their XRD patterns. Furthermore, the XRD results also showed the existence of intrinsic stresses within the films.

Several methods were used to investigate the hydrogen sorption characteristics of our samples. These include thermo-volumetric analysis (HTP), temperature programmed desorption (TPD), thermo-gravimetric analysis (IGA) and DSC (for the Mg powders). The hydrogenation of the samples was confirmed using XRD. Sorption enthalpies of the films were calculated through van't Hoff plots (extracted from PCI diagrams) and were found to be quite high. However, the 40 layer Mg/Ti sample displayed the lowest enthalpy of all. This was attributed to the increased

influence of the cooperative phenomena when increasing the number of layers within the multilayer structure. The sorption kinetics were also investigated showing the 40 layer Mg/Ti sample with the fastest kinetics of hydrogen absorption while the 20 layered sample exhibited the fastest desorption kinetics of all samples. Finally, the TPD results showed a possible presence of the metastable γ-MgH_2 phase which has been suggested to further enhancing the hydrogenation/dehydrogenation properties of Mg.

Chapter 1

Introduction

1.1 Towards a Hydrogen Economy

Energy has always played an essential role in the development of societies empowering technology and transportation networks. The consumption of a significant amount of energy is required to provide basic living conditions of developed countries (heating, transportation, lighting, etc.). Since the Industrial Revolution, this consumption has been mainly fuelled by the burning of fossil fuels in the form of coal, oil and natural gas. The burning of these fuels causes the emission of greenhouse gases (CO_2, N_2O, CH_4, etc.) which are highly linked to the catastrophic effects of global warming. In addition to this, the fossil fuel reserves are decreasing while the demand for energy is rapidly rising. Climate change, the depletion and geographical segregation of fossil fuel resources, health related issues as well as energy poverty constitute the driving forces towards the pursuit of alternative energy resources. An ideal solution would be the use of renewable energy resources (solar, wind, etc.) combined with nuclear power generation, in order to satisfy the world's growing energy demands. Due to the inherent nature of renewable energy resources being intermittent, there is a need to store any surplus energy produced in order for it to be utilised during times of high energy demand [1].

Hydrogen has a great potential for being used as an alternative energy carrier to fossil fuels. Throughout history, the movement towards the use of fuels with decreasing carbon content is evident. Pure hydrogen, free from carbon can provide sufficient energy for everyday use such as lighting and transportation. Combined with oxygen inside a fuel cell, it produces electricity with the only by-product being pure water thus causing zero carbon emissions. Moreover, it is abundant (e.g. within water) and evenly distributed throughout the world providing security in energy. Hydrogen also possesses a high energy content per weight of 120 MJ/kg almost three times of that of petrol 44 MJ/kg [2]. Conversely, even though hydrogen is abundant, in nature it only occurs in chemical compounds such as water or hydrocarbons, thus requiring an efficient and environmentally friendly method of producing pure H_2. Another disadvantage is that in terms of energy content per unit volume, hydrogen exhibits a low capacity (e.g. liquid hydrogen: 8 MJ/l) compared to that of petrol 32 MJ/l causing difficulties in storing hydrogen [2]. In order to move towards a hydrogen based economy a suitable infrastructure is also required for the distribution of hydrogen to the point of utilization.

Hydrogen can be used in both static and mobile applications in which fuel cells offer a very attractive environmentally friendly energy source. To summarise, key elements towards a hydrogen economy would be the development of methods and means of production, storage, transmission and usage of hydrogen.

1.2 Hydrogen Storage

Unlike electricity the production of which is directly linked to its usage, hydrogen can be stored to be used when necessary. As previously mentioned, storing hydrogen is a great

challenge due to its low volumetric energy density. This causes many problems especially in mobile applications due to spatial limitations (Fig. 1.1). Notably, 1 kg of H_2 gas occupies a volume of $11m^3$ under ambient conditions [3].

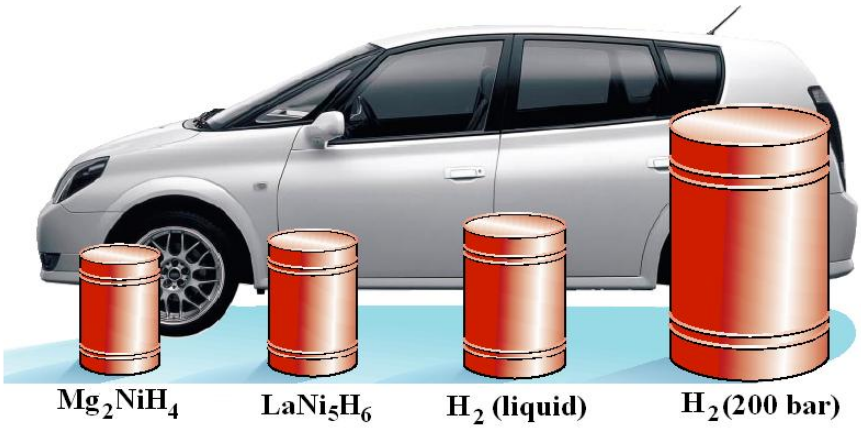

Fig. 1.1: Comparison of the volume required by different methods to store 4 kg of hydrogen.

Hydrogen is mainly stored in the following forms:

- Compressed gas
- Liquid hydrogen storage
- Solid state storage

1.2.1 Compressed hydrogen gas

One of the most common ways of storing hydrogen today is in high pressure gas cylinders. Hydrogen is compressed at high pressures in order to improve its energy density. This technology requires special structure design as well as choice of materials to ensure robustness of the cylinders. Conventional high-pressure steel cylinders store hydrogen at 150 bar, while novel ones made of fibre-reinforced resin have reached pressures up to 700 bar [4]. Issues related to this form of storage are matters of weight and volume of the tanks,

conformability, costs of manufacturing, high energy cost of compressing the gas as well as safety issues.

1.2.2 Liquid hydrogen storage

Liquefying hydrogen offers the advantage of increased volume % storage capacity compared to compressed gas, thus increasing its energy density. At cryogenic temperatures (21.2 K) and atmospheric pressure liquid hydrogen can be stored in cryogenic tanks [3]. The process of liquefaction requires a great amount of energy which is up to 30% of the heating value [4]. Apart from weight, volume and cost issues of the tanks, another matter that has to be considered is hydrogen 'boil off' as the hydrogen evaporates; this can be minimised by employing specially designed tanks.

1.2.3 Solid state hydrogen storage

An alternative storage technique is to use materials which absorb (or adsorb) large amounts of hydrogen at lower pressures; thus reducing the energy required compared to compressing or liquefying the hydrogen. In addition the safety concerns associated with conventional storage methods (high pressure & boil off) are not an issue. This type of storage can be divided into three main areas:

• Porous and high surface area materials: Physisorption of the hydrogen molecules, due to weak Van der Waals interactions, onto the surface of a solid is another possible solution for hydrogen storage. These materials should possess large surface areas in order to increase the amount of hydrogen stored. Low temperatures (-196˚C, liquid nitrogen) are also required due to the weak nature of Van der Waals interactions. Carbon based structures such as activated

carbon and carbon nanotubes can be used in this storage method. Zeolites, metal organic frameworks, as well as porous polymers can also be used as adsorption substrates.

• Metal hydrides: Hydrogen reacts at high temperatures with many metals and their alloys forming metal hydrides. Unlike porous and high surface area materials, where hydrogen molecules are physically adsorbed on the surface, in this storage method hydrogen creates chemical bonds with the metal host. Metal hydrides are a suitable alternative mean for storing H_2 as it is possible to achieve high volumetric and mass densities as well as long term stability [5]. Analytic discussion on the mechanism of hydride formation will be presented further on.

• Complex hydrides: Light elements from groups 1, 2, and 3 of the periodic table (e.g. Li, Mg, B, Al) interact with hydrogen forming stable complex hydrides. During absorption complex hydrides, contrary to metal hydrides, change to an ionic or covalent compound. This storage method presents very high gravimetric and volumetric densities due to the use of light weight metals, as well as their capability of storing usually two hydrogen atoms per metal atom [3]. However, due to the strong nature of the bonds, kinetics are very slow and high temperatures (200-300˚C) are required to achieve hydrogen desorption. Most important examples of complex hydrides are types of alanates (AlH_4), amides (NH_2), and borohydrides (BH_4). The highest gravimetric density at room temperature known today is 18wt% H_2 for $LiBH_4$ [6].

A solid state hydrogen storage method requires certain features in order for it to be a viable storage method. These include, high gravimetric and volumetric hydrogen storage capacities

(>6.0wt%), practical operating pressures and temperature ranges, favourable kinetics for hydrogen absorption and desorption, reversibility and repeatability of the process, relatively low cost, and for it to be safe [7].

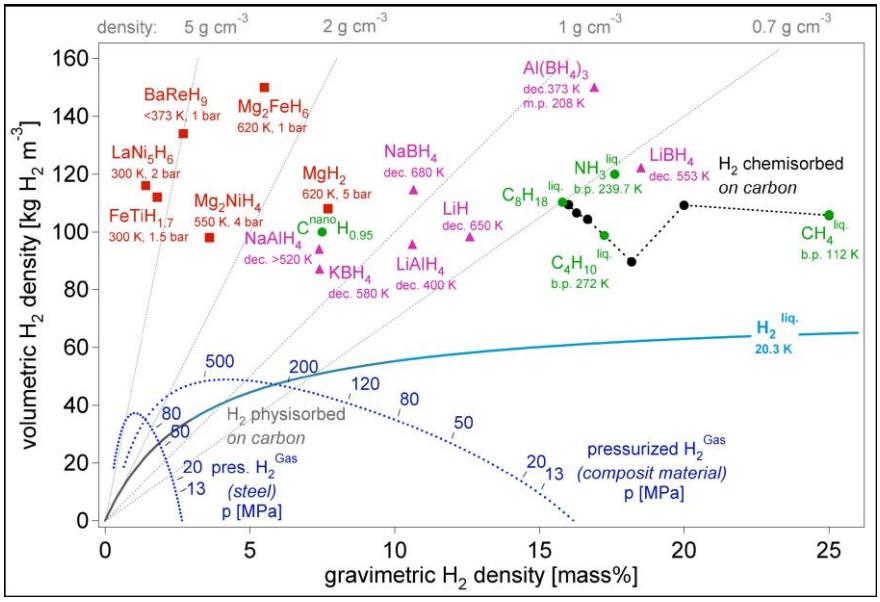

Fig.1.2: Stored hydrogen per mass and per volume, comparison of metal hydrides, carbon nanotubes, gasoline and other hydrocarbons.

Figure 1.2 presents a comparison of gravimetric and volumetric densities of various types of hydrogen storage methods. An ideal method would be placed in the upper right section of the graph possessing both high volumetric and gravimetric densities.

1.3 Metal Hydrides

1.3.1 Hydrogen Absorption and Desorption in Metal Hydrides

As discussed earlier, hydrogen may be stored, under certain conditions of pressure and temperature, as a solid in the form of a metal hydride. Metal hydrides provide an efficient and safe means of hydrogen storage whilst high volumetric as well as gravimetric densities

are achievable from their formation. During hydrogen absorption, H_2 molecules are first physically absorbed through Van der Waals interactions by the metal surface. At the surface of the metal, the H_2 molecules dissociate into 2 hydrogen atoms which are then chemically absorbed and diffused into the subsurface and bulk of the metal forming a solid solution (α-phase). During hydrogen diffusion the atoms move through the octahedral and tetrahedral interstitial sites finally causing the formation of a hydride phase (β-phase) by nucleation and growth [3].

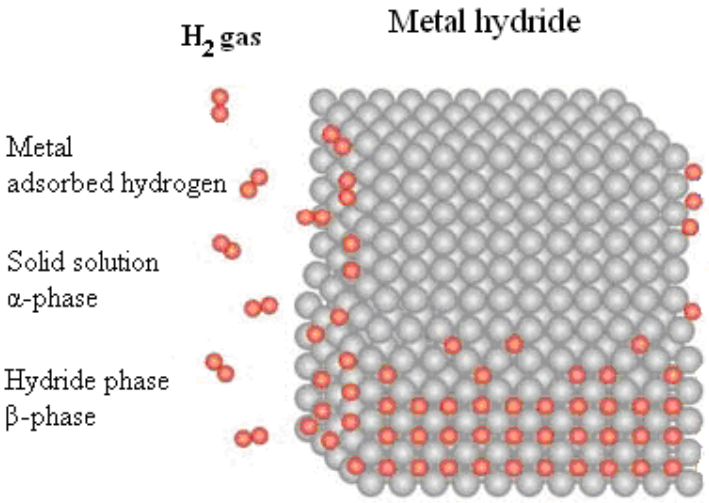

Fig. 1.3: Model of a metal atom structure with H atoms on interastitials and H_2 molecules at the surface. Hydrogen atoms from physisorbed hydrogen molecules on the left hand side.

In the case of desorption the opposite process occurs. At first the metal is formed and the hydrogen atoms then diffuse to the metal surface. The atoms then recombine to hydrogen molecules, finally being physically desorbed. In figure 1.3, the process of hydrogen absorption and desorption can be observed. During hydrogen absorption the lattice of the metal host expands by up to 10-20% [8]. As a result, the induced internal strain and lattice defects may cause decrepitation of brittle metal hosts.

Figure 1.4 presents the potential energy curves according to the distance of the hydrogen gas from the metal surface [8]. Away from the metal surface the potential energy of the atomic hydrogen is larger than that corresponding to molecular hydrogen during dissociation. Approaching the interface molecular hydrogen is physically adsorbed from the metal (lowest point of the curve).

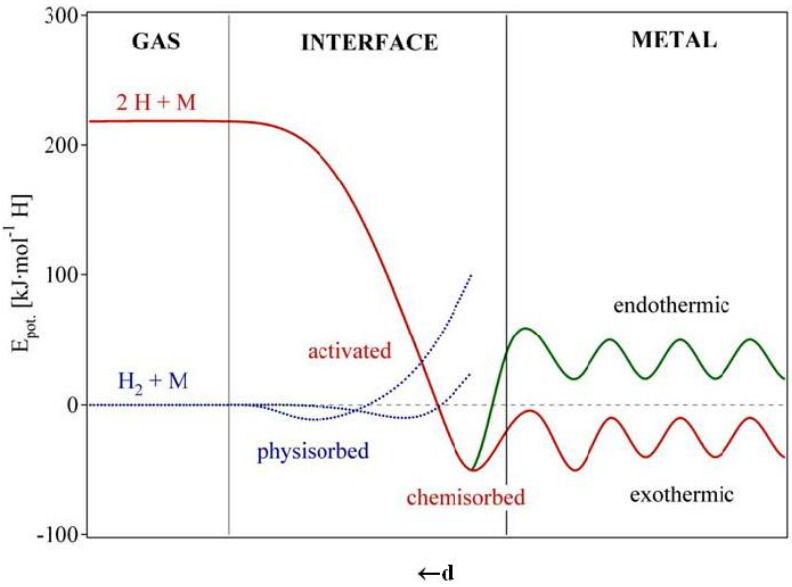

Fig. 1.4: Diagram of the potential energy according to the distance of the hydrogen gas from the metal surface.

For smaller distances the potential energy of molecular hydrogen rises infinitely due to the metal surface while the curves of atomic and molecular hydrogen intersect at a transitional point. At this point, an energy barrier, which depends on how active the metal surface is, has to be overcome in order to achieve dissociation of the molecular hydrogen into hydrogen atoms. These atoms locate suitable positions and diffuse into the metal bulk, thus forming the hydride phase.

1.3.2 Thermodynamics of Metal Hydrides

Isotherm curves of pressure-versus-composition describe the thermodynamic behaviour of hydride formation from gaseous hydrogen. Examples of pressure-concentration-temperature plots are shown in figure 1.5. At low concentrations of hydrogen, there is an increase in hydrogen pressure initiating the formation of the solid solution (α-phase), as the concentration of hydrogen continues to increase a plateau appears where both the α and β phases are present. In the pure β-phase region the isotherms display again a steep rise in pressure corresponding to the increasing hydrogen concentration. The plateau pressure is temperature dependent, while above a critical temperature, T_c, the plateau disappears. This indicates an end to the two-phase region and a continuous transition from the α to β phase. The plateau pressure is associated to changes in thermodynamic properties of enthalpy and entropy according to van't Hoff's equation:

$$\ln\left(\frac{p_{eq}}{p_{eq}^{0}}\right) = \frac{\Delta \mathrm{H}}{R}\frac{1}{\mathrm{T}} - \frac{\Delta S}{R} \tag{1.1}$$

where, ΔH is the enthalpy of formation (kJ mol^{-1}) H_2, ΔS is the entropy of formation in J K^{-1} mol^{-1} H_2, R is the gas constant and T is the absolute temperature. The change of the entropy relates to the transformation of molecular hydrogen gas to dissolved atomic hydrogen; this value is negative for all metal-hydride systems and almost equal to -130 $JK^{-1}mol^{-1}$ [3]. Equation 1.1 displays a linear form when plotted as $\ln p_{eq}$ versus 1/T, the slope of the van't Hoff plot gives the normal difference in enthalpy divided by the gas constant, R. The value of the enthalpy change, ΔH_0, is dependent on the type of metal hydride and describes the stability of the metal-hydrogen bond, an important element for the characterization of metal hydrides. Hydride stability relates to the heat that has to be provided in order to achieve hydrogen sorption for a certain pressure.

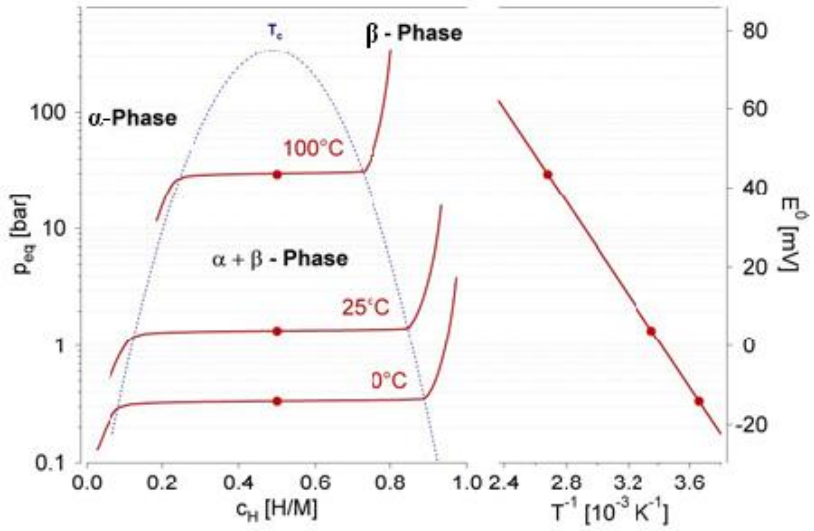

Fig. 1.5: On the left hand side, examples of pressure-composition-isotherm (PCI) curves and on the right hand side, the resulting van't Hoff plot.

Hydrides that feature a larger slope of the van't Hoff plot have a more negative ΔH_0, and therefore, require greater heat in order to achieve the reversible process of formation and decomposition of the metal hydride. The formation of a metal hydride during hydrogen absorption releases a significant amount of heat due to the exothermic nature of the reaction, while the same heat is required to desorb hydrogen from the metal hydride (endothermic reaction) [3].

The pci diagrams in figure 1.5 represent an example of an ideal metal hydride. In this case, the plateau of the two phase region is completely flat and represents both absorption and desorption of hydrogen. Real metal hydrides most often exhibit a slope in their plateaus as well as a plateau-pressure difference between absorption and desorption causing a hysteresis between the respective curves of the PCI diagram (Fig. 1.6). Although, the origin of hysteresis is not yet completely understood, it has mainly been attributed to the various stress states caused by expansion of the metal lattice during (de)hydrogenation [9-11]. The pressure

of absorption is generally higher than that of desorption because of the extra energy required to overcome constraints related to lattice expansion during hydrogenation.

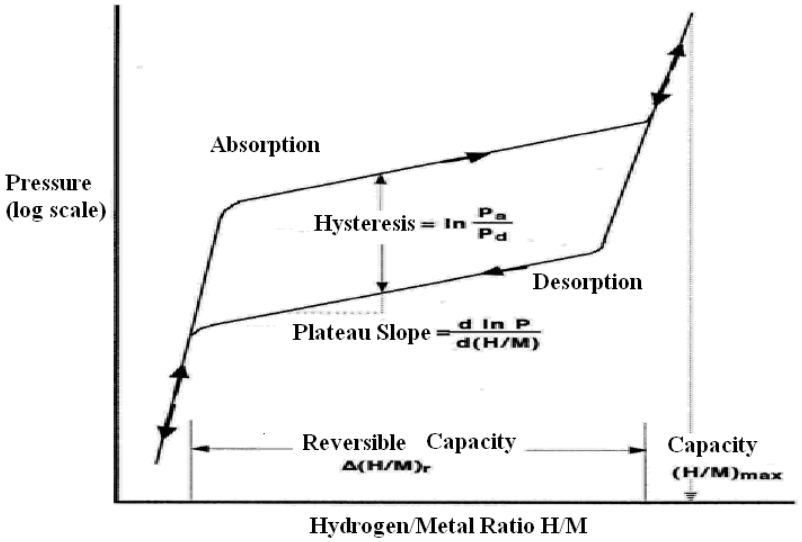

Fig. 1.6: A generic metal hydride isotherm. The hysteresis, plateau slope, capacity and reversible capacity are also exhibited.

Both hysteresis and plateau slopes indicate irreversible energy losses in the vicinity of the growing metal hydride, thus posing a serious problem during absorption-desorption cycling [9,10]. These metal hydride features depend on chemical composition and pressure-temperature conditions and can be minimized through metal additives and heat treatment.

1.3.3 Criteria for selecting a Metal Hydride

In order to achieve optimum hydrogen storage, metal hydrides should possess several important features. These include large hydrogen storage capacity per unit mass and unit volume (determines the amount of available energy), reversibility and fast kinetics, low dissociation temperature and moderate dissociation pressure, minimal activation of the metal hydride surface (enhances the process of hydrogen absorption). Low heat of formation of the metal hydride is also necessary in order to minimise the energy required for hydrogen release

meanwhile minimizing the heat that has to dissipate during the exothermic hydride formation. As mentioned earlier, small hysteresis and minimal plateau slope (limited energy loss during hydrogenation/dehydrogenation) of the PCI diagrams are desirable, in addition to closed absorption/desorption curves in order to avoid remaining H_2 inside the hydride during desorption. Finally, a metal hydride should posses chemical stability, be of low cost, light weight and posses a long life cycle [6,12].

Chapter 2

Literature Review

2.1 Magnesium as a Hydrogen Storage Material

Magnesium has been widely investigated as a possible hydrogen storage material, as it includes several desirable characteristics crucial for its applicability. It is light-weight, naturally abundant, and is relatively low-cost. Magnesium hydride, MgH_2, is especially interesting due to its very high reversible hydrogen capacity reaching up to 7.6 wt% [13]. On the other hand, Mg forms a very stable hydride due to the strong Mg-H ionic bonds, resulting in a relatively high enthalpy of formation, ΔH = -75 KJ/mol [14]. This means a high temperature (350°C) is typically required to achieve hydrogen desorption at a high enough pressure (> 1 atm) [13]. Another problem with Mg is that it easily forms an oxide (or even hydroxide) when exposed to air due to magnesium's high affinity for oxygen [15]. The oxide layer that forms on the metal surface acts as a diffusion barrier, resulting in very low rates of hydrogen absorption/desorption [16]. In addition to this, the oxide layer limits the number of dissociation sites for H_2, further reducing the hydrogen uptake rate [13]. Another feature that negatively affects the sorption kinetics is that hydrogen molecules do not readily dissociate on a 'clean' magnesium surface [16]. Finally, the initially formed magnesium hydride phases create a 'surface shell' which blocks further hydrogen uptake. This delays diffusion of the hydrogen atoms inside the metal bulk [6]. Due to kinetic reasons, the hydrogenation reaction entirely diminishes once the hydride layer exceeds 30-50 μm [16]. This indicates that

complete hydrogenation of magnesium is almost impossible, even at high pressure and temperatures.

To summarize, the problems associated with magnesium as a hydrogen storage material are:

1. The stability of the MgH_2 phase
2. The formation of a surface oxide(s)
3. Slow diffusion of hydrogen through MgH_2
4. Slow dissociation of hydrogen at the metal surface

Possible solutions to the above problems have been widely investigated some of which include the development of a nanocrystalline material; introduction of a catalyst to promote the dissociation of hydrogen; activation to crack oxide layers; and by alloying with other metals to destabilize the hydride.

2.2 Influence of microstructure and particle size on the sorption kinetics of magnesium based hydrides

An approach to improve the sorption kinetics of magnesium based hydrides is modification of the microstructure and particle size of the material. By reducing the grain or crystallite size of hydrogen storage materials, we are able to achieve a lower packing density of the metal atoms. This enhances hydrogen diffusion as atoms generally move much faster along the grain boundaries than through the metal lattice [16]. Additionally, grain boundaries act as favourable nucleation sites for the formation and decomposition of the hydride phase. The outer dimension of the material, for example the particle size in case of powdered materials, also affects the sorption kinetics as it determines the surface area. Large specific surface area is attained through small particle size, increasing the rate of surface reaction with hydrogen.

The surface area is also related to the length of the diffusion paths of hydrogen into the metal bulk.

The development of nano-structured metal hydrides is an approach to benefit from the previous characteristics and overcome the drawbacks of bulk magnesium based hydrides. Nano-structured metal hydrides can be developed in different forms (nano-powders, thin films, etc.) by using methods such as ball-milling, sputtering, vapour condensation, laser ablation, etc.

2.2.1 Magnesium based powders

Magnesium powders possess many advantages compared to magnesium in its bulk form, since they have a larger surface-to-volume ratio. On the other hand, the smaller particle size and therefore larger surface area of the Mg powder causes the material to be more susceptible to oxidation. Hydrogen is easily physisorbed and dissociated on the increased metal surface of the Mg powder, while nucleation of the hydride is at the same time increased. The small powder size may also be a solution to the problem of the 'blocking' layer of MgH_2 as the Mg powder can be fully hydrogenated when the average powder radius is smaller than 30-50 μm, or a diameter of about 60-100 μm [16]. Magnesium powders can be produced using various methods. Ball milling has been proven to be an effective way of activating and improving hydrogen sorption properties [16-18]. The main effect of this method is the increased surface area which results from decreasing the crystallite size of the Mg powders. Ball milling also results in 'cracking' of the oxide layer of magnesium. According to Hanada et al, the crystallite size of the MgH_2 gradually decreases with increasing milling time down to 7-8 nm after 3 h of milling [18]. For longer milling time the

grain size remains almost unchanged. The effect of the small grain size on hydrogenation kinetics has been intensively studied and it has been shown that both rates of absorption and desorption of hydrogen are enhanced [16,19,20]. The enhanced hydrogenation results from the combined action of many factors. As previously stated, ball milling provides several defects and grain boundaries near the powder surface which act as hydride nucleation sites. Furthermore, hydrogen diffusion is much faster along the grain boundaries, Mg-MgH_2 interface, as well as the imperfections, rather than through the metal lattice [16,19].

Mechanical milling of Mg under a hydrogen atmosphere also causes a partial formation of the metastable orthorombic γ-MgH_2 phase. This happens when the hydrided β-phase with tetragonal structure is subjected to high compressive stress. At this point it is worth noting that magnesium as well as the solid solution α-phase have an hcp crystal structure. According to Gennari et al, the γ-MgH_2 and β-MgH_2 mixture shows a synergetic effect during hydrogen desorption [21]. This effect causes a decrease in the β-MgH_2 desorption temperature [21,22]. The improvement of the hydrogen desorption properties becomes more significant as the milling time increases from 35 to 100 h, due to better phase intermixing of γ- and β-hydrides [21].

Another important parameter that improves hydrogenation is the particle size of magnesium powder which determines its specific surface area; an increase of which leads to a faster rate of surface reaction and also shortens the length of diffusion paths for hydrogen [23]. Mechanical milling of MgH_2 provides a particle size down to 300 nm, while in most cases problems of agglomeration and impurities occur [24]. Other methods such as gas phase condensation produce nanomaterials with smaller particle size (50-200 nm). Theoretical

studies have indicated that MgH_2 is less thermodynamically stable as particle diameter decreases below 2 nm. This is likely to lower the enthalpy of formation of magnesium hydride, thus causing a decrease in the desorption temperature. Unique properties, such as high reversible hydrogen storage at low temperatures as well as hydrogen desorption at 85°C, have been observed for Mg nanoparticles (5 nm) prepared by electrochemical synthesis, demonstrating the correlation between particle size and sorption properties [24].

2.2.2 Thin film Mg hydrides

Nanostructured metal hydrides may also be manufactured in the form of thin films. The production thin films offer a number of advantages compared to lengthy ball milling procedures or complicated chemical synthesis. These include control over the layer thickness and a flexibility to tailor both the composition and the degree of crystallization of the metal film [25]. Parameters such as sample geometry, particle size and morphology, oxygen content and material preparation may strongly influence the hydrogenation-dehydrogenation mechanism. Films have a simple geometry and therefore offer a suitable way to study the hydrogenation mechanism and properties of metal hydrides.

The study of pure magnesium films has been carried out by several research groups [26-29]. Leon et al. were able to successfully store 7.5 wt% of hydrogen inside 30-μm thick air-exposed Mg film samples [26]. Both absorption and desorption were achieved at quite a high temperature (350°C). Lower temperatures of hydrogen absorption (about 130°C) were reported for 5 μm thick Mg films using high-flux ion irradiation [28]. This temperature was significantly lower than that required for MgH_2 synthesis using Mg powder in hydrogen atmosphere. Controllable high flux irradiation creates many grain boundaries, defects,

disorder or strain, thus enhancing hydrogen diffusion [28]. A characteristic of magnesium films is that their growth has been proven to be highly oriented along one direction as the highest intensity in XRD profiles of Mg films appears for the Mg(002) diffraction reflection [26-28]. Moreover, analysis of diffraction profiles after hydrogenation reveal that MgH_2 also grow along a preferred orientation [26].

The hydrogenation properties of pure magnesium nanostructured materials may be further improved by adding certain materials which act as catalysts or alloying Mg with suitable additives. In the case of Mg thin films the development of multilayer structures have also been studied for enhancing hydrogen absorption and desorption.

2.3 Addition of catalysts

An important approach to improve the sorption properties of hydrides, is the application of suitable catalysts. As previously mentioned, hydrogen absorption of pure magnesium is limited due to the low probability of absorption (10^{-6}) of a hydrogen molecule on the Mg surface [30]. Several attempts have been made to enhance surface kinetics of Mg hydrides by affecting the probability of hydrogen dissociation with the use of metallic catalysts [31]. Elements mainly from groups of transition metals (Ni, Pd, Ti etc) and transition metal oxides have been proven to act as effective catalysts [30-36]. Applying large amounts of a catalytic material and fully covering the surface of magnesium does not necessarily imply effective catalysis. Instead, evenly distributing small particles or a thin layer of a catalyst on the outer metal surface is sufficient [16,33]. Titanium is an example of an excellent catalyst for promoting the reaction of hydrogen dissociation on the magnesium surface thus enhancing the sorption kinetics (figure 2.1) [36].

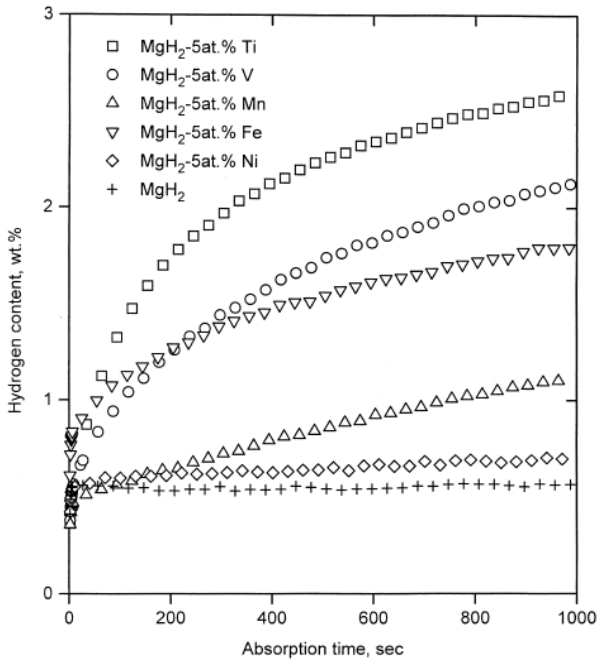

Fig. 2.1: Hydrogen absorption curves (1.0 MPa H_2 pressure) of Mg–transition metal composites at 302 K [36].

The problem of magnesium oxidation may also be diminished through the use of catalysts. Many research groups apply a thin overlayer of palladium on magnesium films to prevent the samples from oxidising. This is due to the easy decomposition of palladium oxide during exposure to hydrogen [6]. Zaluski et al. have also reported that the presence of a small amount of Pd (1 wt%) as a catalyst in nanocrystalline Mg offsets the negative effects of surface oxidation and eliminates the need for activation, meanwhile the kinetics of hydrogen absorption are dramatically enhanced. A disadvantage of applying a metal catalyst is the reduced wt% of absorbed hydrogen, due to an increase in the overall weight of the Mg-catalyst complex, as well as the increased expenses in the case of Pd or other PGMs (platinum group metals) [16].

2.4 Alloying of magnesium

A different strategy is to decrease the sorption enthalpy of magnesium and therefore the temperature of desorption, by the formation of Mg-based compounds through the alloying of magnesium with 3d transition metals [5,37,38]. Mechanical alloying is the most common method used for producing these materials, with the aim of destabilizing the MgH_2 phase [39-40]. Some elements, such as titanium do not form an alloy with magnesium by using conventional melting methods, therefore considerable research has been carried out to find alternative approaches. A major drawback of Mg-Ti alloys is that during hydrogenation they decompose forming MgH_2 and TiH_2 instead of a ternary hydride, and as a result destabilization of MgH_2 is not achieved [41]. The use of high pressures in the GPa range and thin film processing have been shown to produce ternary Mg-based hydrides (e.g. Mg-Ti-H) with significantly lowered hydrogen bonding enthalpies [42,43].

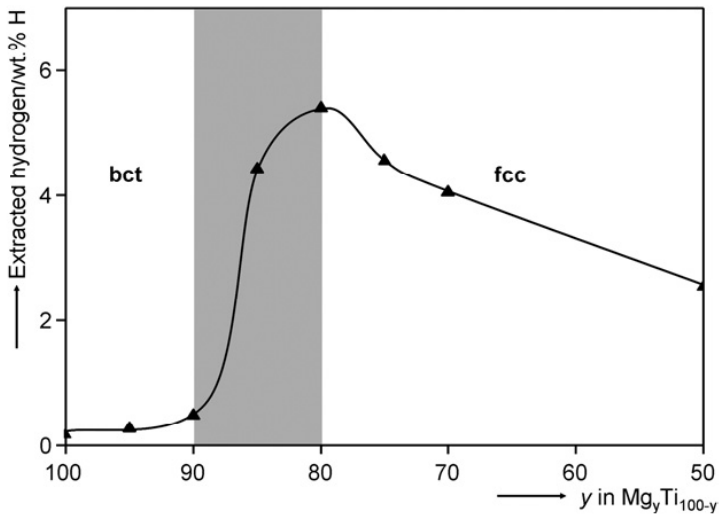

Fig. 2.2: Discharge capacities for fully hydrided $Mg_yTi_{100-y}H_x$ electrodes with varying composition. The Mg content (y) was varied from y = 50 to 100 at.%. Indicated are the regions where hydrides with bct ($y \geq 90$) and fcc ($y \leq 80$) structures are found. Between 80 and 90 at.% Mg the coexistence of both structures can be found [44].

Vermeulen et al. have reported low temperature hydrogen reactions in metastable Mg-Ti thin films [43]. It is worth noting that Mg_yTi_{1-y} (y=0.80) thin films exhibit an excellent rate-

capability along with a superior hydrogen storage capacity [43]. In addition to this, it has been shown that under certain conditions, Mg-Ti can form a new single phase fcc-structured hydride, upon hydrogenation [43,44]. The fcc Mg-Ti lattice has been proven to favour fast hydrogen insertion, whereas the common bct structure of MgH_2 strongly inhibits hydrogen transport (figure 2.2) [44].

2.5 Thin Film Multilayers

The production of magnesium thin films by using magnetron sputtering techniques (RF or DC) has been an emerging field of research for tackling the problems of MgH_2 as it allows some control of the structure and thickness of the film layer to nanometre scales [45-47]. The formation of thin films offers a different path of achieving a high surface area that will enhance hydrogen storage properties of magnesium, while the application of catalytic thin film overlayer provides additional benefits by enhancing the sorption kinetics. Moreover, films constitute fine model systems for researching the relation between microstructure and the properties of Mg-based hydrogen storage alloys [48,49].

The formation of a multilayered thin film complex has been shown to lower the temperature of hydrogen desorption for magnesium as well as boost the sorption kinetics [45,46,50]. This structure is obtained by alternating between magnesium and catalytic layers during the thin film deposition procedure. The hydrogen storage properties of multilayered thin films have been widely investigated. Fujii et al. have reported a tri-layered (Pd/Mg/Pd) hydrogen storage system which absorbs ~5 wt% hydrogen at 100°C under 1bar of hydrogen and is fully dehydrogenated at about 90°C [45]. The authors suggested that the reduced temperature of hydrogen desorption presented for Mg/Pd thin films is due to a phenomenon developed in

nano-composite interface regions between the Pd and Mg layers and is referred as the cooperative phenomena [45,46].

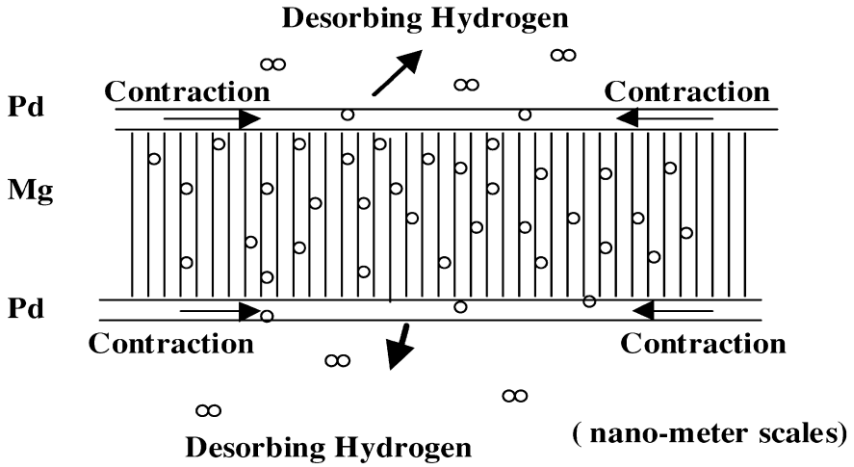

Fig. 2.3. Schematic diagram of the cooperative phenomena on a hydrogenated Pd/Mg/Pd film [46].

Figure 2.3 illustrates a schematic diagram of the cooperative phenomena. When the temperature of the sample is increased hydrogen is initially desorbed from the Pd films because of the lower desorption temperature of Pd compared to Mg. This causes contraction of the Pd films thus inducing compressive stress on both sides of the Mg layer. The authors contend that the stress strongly influences the Mg film by destabilizing the absorbed hydrogen which then desorbs at a lower temperature [45,46].

2.5.1 Thickness of layers

An important parameter that affects the 'performance' of hydrogen storage multilayered structures is the thickness of the Mg layer. Higuchi et al. have reported that increasing the thickness of the Mg layer, from 25 to 800nm, in Pd/Mg/Pd (RF sputtered) samples results in a rapid decrease in the temperature of dehydrogenation [46]. This is confirmed by the thermal desorption spectroscopy (TDS) profiles in figure 2.4 which show a shift of the peak position to lower temperatures with increasing the thickness of Mg [45]. On the other hand,

no dependence on the thickness of Pd film has been observed for the hydrogen sorption properties of Mg [45].

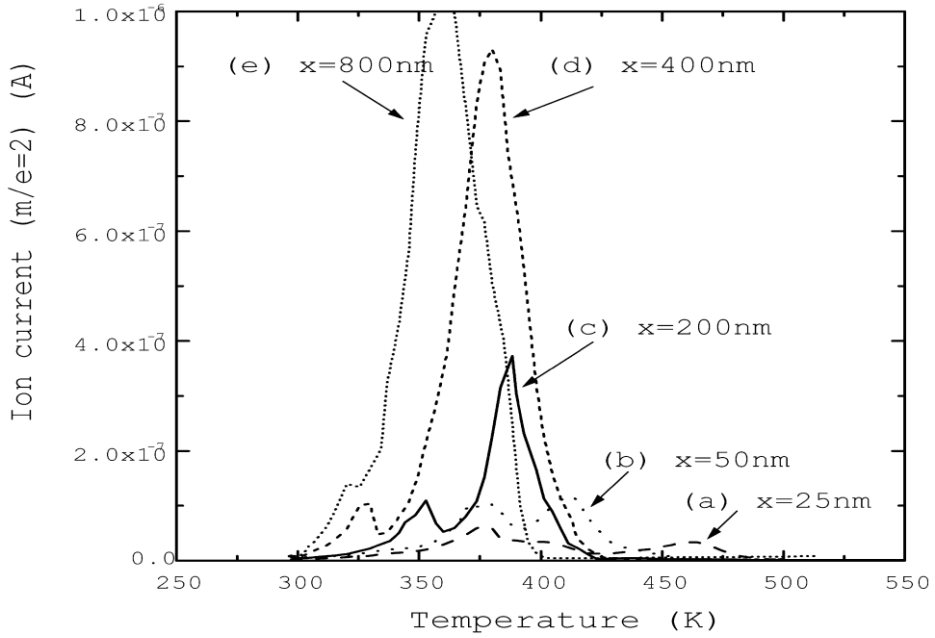

Fig. 2.4: TDS spectra of several hydrogenated Pd (50nm)/Mg(x nm)/Pd (50nm) films with x = 25, 50, 200, 400 and 800nm [45].

The amount of hydrogen absorbed from three-layered Pd/Mg/Pd samples was reported to be ~5 wt% and almost independent of the thickness of Mg [45,46]. This is in contrast with results for RF sputtered Pd/Mg bi-layers which exhibit a reduction in hydrogen content with increasing thickness [45]. On the other hand, Yoshimura et al. have reported an increase in hydrogen content subject to an increase of the Mg film thickness in DC sputtered Pd/Mg [47]. These results were obtained through monitoring reflectance changes of the samples upon hydrogenation and are presented in figure 2.5. A small change in the sorption kinetics is shown with an increase in the thickness of Mg.

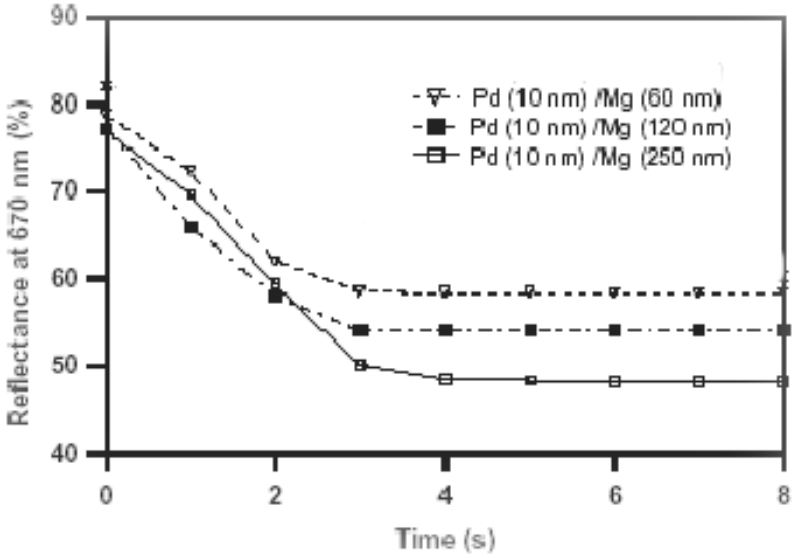

Fig. 2.5: Time evolution of optical reflectance of Pd capped Mg layers that vary in thickness [47].

According to Fujii et al. the thickness of the Mg layer also influences the level of stress induced upon the Mg surface [45]. Multilayer films with a thin Mg layer were not shown to peel off the substrate thus causing an anisotropic deformation of magnesium. This gives rise to only a small compression stress on the Mg film plane reducing the magnitude of the cooperative phenomena and therefore the enhancement of the thermodynamics of the system [45]. On the other hand, the thin film samples that peeled off the substrate were liable to degradation.

2.5.2 Number of layers

Varying the number of layers of a multilayered thin film structure has been studied as an alternative way to improve hydrogen storage properties. Krozer and Kasemo found that the majority of absorbed hydrogen atoms are trapped in the Pd/Mg interfaces, where defects are concentrated due to the Pd-Mg lattice mismatch [51]. Figure 2.6 illustrates the dramatic increase in the hydrogen uptake of the Pd/Mg/Pd/Mg sandwich structure compared to simple Pd capped Mg films. This is attributed to the larger number of Pd/Mg interface regions in the

multilayered sample. On the other hand, the presence of hydrogen in the Pd/Mg interface has been reported to prevent hydrogen interdiffusion [52]. In agreement with Krozer and Kasemo, Higuchi et al. have reported that the hydrogen uptake in the Mg film of the Pd/Mg/Pd structure is almost doubled compared to that of Pd/Mg bi-layers with the same thickness of the Mg film (800 nm) [46].

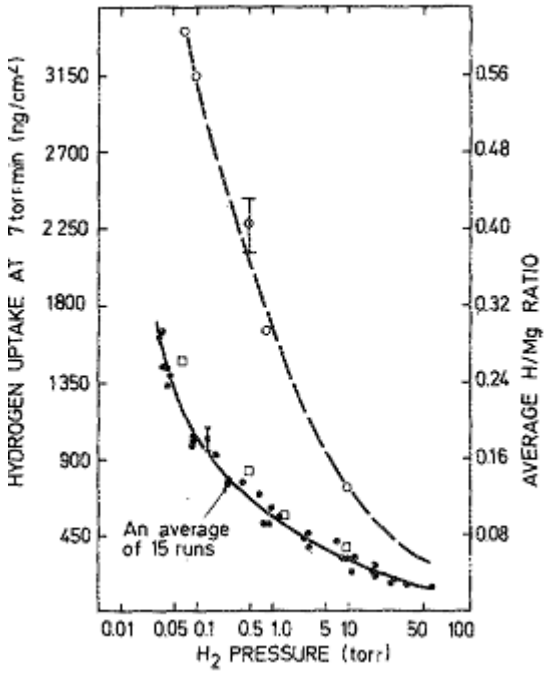

Fig. 2.6: The total hydrogen uptake measured with a quartz-crystal microbalance at different pressures at 293K. The open circles represent Pd/Mg/Pd/Mg/Pd film with Pd = 130A and Mg= 3900A. The open squares are data for Pd covered Mg of 390nm thick. The filled circles are data for Pd covered Mg layer of 780nm [51].

TDS measurements have shown a dependence of the Mg dehydriding temperature on the number of layers in a multilayered structure [45]. The TDS spectra of multilayered Pd/Mg thin films are presented in figure 2.7 as a function of the number of layers. The temperature of hydrogen desorption clearly drops to the lower temperature region with increasing number of layers. This behaviour is attributed to an additional stress applied on the Mg surface from the Pd films according to a multiple effect of the cooperative phenomena.

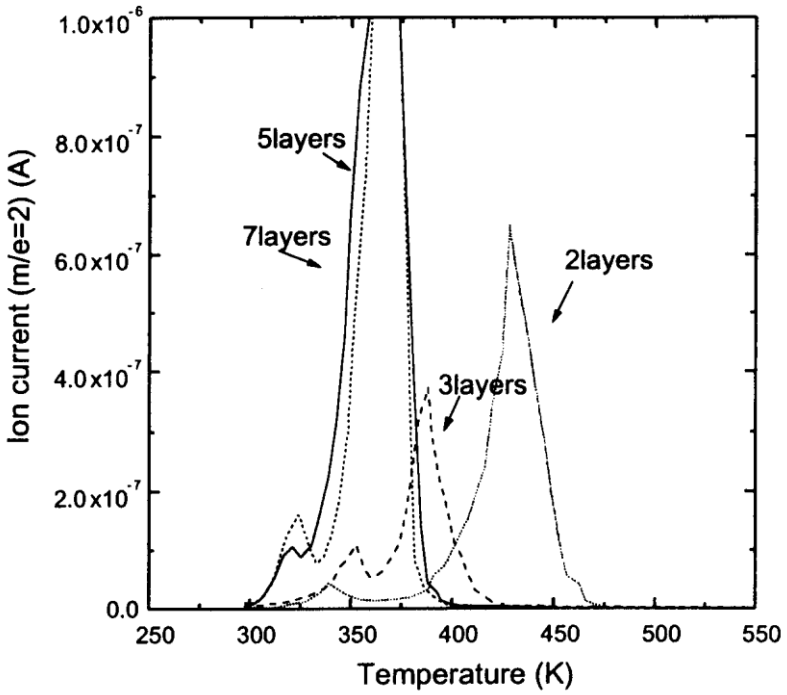

Fig. 2.7: TDS profiles of multi-layered Pd(50 nm)/Mg(200 nm thin films as a function of the number of layers [45].

2.5.3 Interface region

The existence of an intermixed zone between layers has also been shown to improve the hydrogen sorption properties in terms of the desorption capacity and the absorption/desorption cycle life of the film [53]. Singh et al. have reported alloying at the Pd/Mg interfaces of multilayered thin film structures for temperatures above 247°C [25]. This result might be beneficial in the case of Ti/Mg multilayered films, assuming that the formation of such an alloy enhances the hydrogen sorption properties of Mg (as discussed earlier in paragraph 2.4).

2.6 Aim of project

In this chapter, several methods have been discussed which have shown potential in overcoming the major drawbacks that magnesium exhibits as a hydrogen storage material.

These solutions include reducing the particle and grain size of Mg, incorporating a secondary material to act as a catalyst, as well as producing metastable Mg alloys. Moreover, the design of multilayered thin film structures has been proposed to benefit from the combination of the advantages of each of the previous methods in terms of their hydrogen storage properties. Among the various types of multilayers, Pd/Mg has received considerable attention due to reports of promising hydrogen storage characteristics.

This work builds on the aforementioned multilayered thin film theory. We propose an alternative structure consisting of a Mg and Ti multilayered thin film. This novel approach is based on certain assets of titanium which render Mg/Ti a promising hydrogen storage material. These include its light-weight, catalytic action, the ability of forming a metastable Mg-Ti phase, as well as its reduced production cost compared to palladium. In this study, we will first investigate the structural and hydrogenation properties of pure nano-Mg in the forms of powder and thin-film. Next, we will explore the performance of Mg/Ti thin film multilayers with respect to the number of deposited layers of both materials, while preserving the total thickness of Mg within the structure.

Chapter 3

Experimental

3.1 Sample Preparation

3.1.1 DC Magnetron Sputtering of Thin Films

Magnesium/titanium multilayer films were produced by DC magnetron sputtering using a Teer Coatings Ltd UDP 350-4, sputter ion plating system installed at the University of Birmingham in January 2008. The system was supplied with a glove-box attachment allowing the inert transfer of substrates and sputtered samples. Magnetron Sputtering provides the advantage of well controlled production of high quality coatings with excellent adhesion to almost any type of substrate. The Closed Field Unbalanced Magnetron Sputter Ion Plating (CFUBMSIP) system employed to produce the thin film samples was developed and patented by Teer Coatings Ltd. The system uses unbalanced magnetrons arranged such that neighbouring magnetrons are of opposite polarity as illustrated in figure 3.1. In this arrangement the deposition zone in which the substrates are located is surrounded by linking magnetic field lines. This traps the plasma preventing loss of ionising electrons and resulting in significant plasma enhancement.

Glass and stainless steel substrates were pre-cleaned with industrial methylated spirit (IMS) in an ultrasonic bath which were then placed into the coating chamber which was then evacuated. Once a vacuum of $5x10^{-6}$ mbar or lower was reached, a controlled flow of argon

was introduced with the vacuum pumps still running raising the pressure in the system to the level required to operate the magnetrons (~$4x10^{-4}$ mbar). The magnetrons consist of magnets arranged behind the target (a plate of material of which the coating is to be made) creating a magnetic trap for charged particles such as argon ions in front of the target. A negative voltage (typically -300 V or more) is applied to the target resulting in argon ions being attracted to the target's surface.

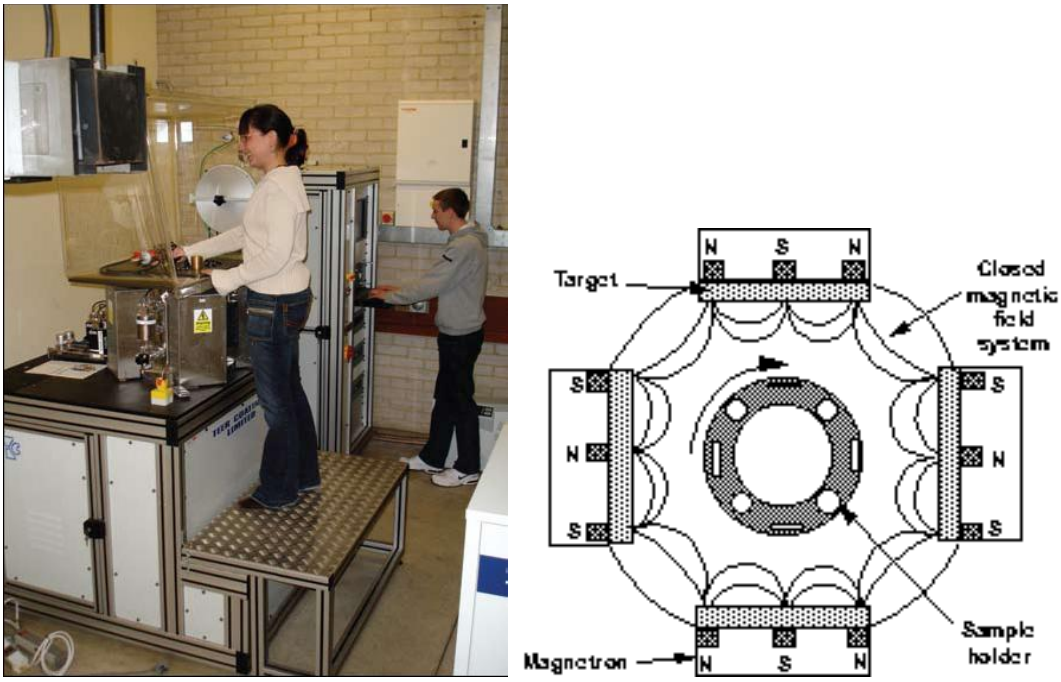

Fig. 3.1: Left: DC Magnetron Sputtering system from Teer Coatings Ltd and Right: arrangement of the magnetrons inside the chamber of the Teer Coatings Magnetron Sputtering system.

When the argon atoms hit the surface of the target two processes take place:

- atoms are knocked out of the target (this is sputtering); these sputtered ions which are not charged thus leave the magnetic trap and form a coating on the substrates.
- the surface may also release electrons which are held within the magnetic trap and are used to produce additional argon ions.

A few tens of volts are also applied to the workpiece thus attracting ions out of the plasma with enough energy to densify the coating and improve the adhesion. The energy of these

ions is fairly low to avoid sputtering off of the coating. By alternating between Mg and Ti targets thin film multilayers were produced.

Samples were also provided by Teer Coatings Ltd; these included pure Mg and Mg/Ti multilayered samples which were sputtered on glass, stainless steel 316 and silicon substrates. These samples were also fabricated by using a CFUBMSIP system. All samples were vacuum packed within 10 minutes of unloading in order to reduce oxidation effects.

3.1.2 Mg powder samples

Magnesium nano-powders (<100nm) were provided by Dr Isaac Chang (Dept. of Metallurgy and Materials) and Metal Nanopowders Ltd. using a technology based on a patented process. This involves the application of a large direct current between two electrodes that are initially in contact and surrounded by a coolant inside a container. An arc column is formed when the electrodes begin to separate the heat of which causes melting and/or evaporation of the electrode (in this case magnesium). The droplets and/or vapour is finally quenched into solid powder particles (<1μm) using the surrounding coolant. A Schlenk line was later used to remove the ethanol (in the School of Chemistry), as the sample provided was in the form of a solution.

Gas atomised powders 500 mesh were supplied by Magnesium Elektron. These spherical powders were produced by spraying molten magnesium of high purity (>99.8%) under the protection of an inert atmosphere. For comparison, magnesium powder of -325 mesh (~ 44 μm) was obtained from Alpha Aesar and MgH_2 powder was obtained from Goldschmidt.

3.2 Material Characterization

3.2.1 Scanning Electron Microscopy (SEM)

The microstructure of the multilayer samples were studied using a JEOL 6060 and a JEOL 7000 Scanning Electron Microscope (SEM) to obtain Secondary Electron images (SEI) and Back Scattering images (BSI). Energy Dispersive Spectrum (EDS) analysis, was also used to investigate the composition of the samples. Films mounted in conducting Bakelite were prepared by grinding on SiC paper to 1200 grit followed by mechanical polishing with 6μm, 1μm and 0.25μm diamond suspension.

3.2.2 X-Ray Diffraction (XRD)

X-Ray diffraction, a non-destructive technique based on Bragg's law, was used in order to study the composition and structural properties of the multilayer samples. At first a monochrome X-ray beam is produced striking the surface of the samples at an angle of θ (Bragg angle). This incident beam is diffracted by the atomic planes of the crystalline sample. The diffracted beam is then monitored by a moving detector measuring the different d-spacings. These are derived from the observed 2θ reflections and through Bragg's equation:

$$n\lambda = 2d\sin\theta \tag{3.1}$$

Where λ is the wavelength, d is the interatomic spacing, θ is the Bragg angle at which one observes a diffraction peak and n is an integer number called the order of reflection. XRD provides a wide range of possibilities when investigating thin film samples (composition, film thickness, lattice strain, orientation, etc.), nevertheless this method presents some difficulties. When examining thin films the results may be highly dependent on the method of fabrication (texture, orientation, induced strain etc.). Moreover, the amount of material (single phase) should be sufficient enough to get high intensity XRD peaks, thus accurate

results. Peak overlay in the XRD patterns may also occur not allowing clear interpretation of the results.

The XRD measurements were performed using a D8 Advance from Bruker equipped with a Cu anode. This uses Cu Kα radiation (λ= 1.5406Å) selected by a Ge crystal monochromator. Measurements were taken over a 2θ range of 5-90°. The films were mounted in an argon filled glove-box, onto a sample holder and pressed flat prior to being covered with Kapton tape in order to minimize oxidation effects. The gas atomised Mg powder sample was mounted in an argon filled glove-box into a sample holder and pressed flat and then scaled with a transparent beryllium dome instead of using Kapton tape. The XRD patterns produced by both the Kapton tape and beryllium dome were known prior to the sample measurements and were taken into account while analysing the XRD data.

3.2.3 Differential Scanning Calorimetry

A Netzsch DSC 204 high pressure (up to 150bar) Differential Scanning Calorimeter (DSC) was used to measure the thermodynamic properties of the samples. By monitoring the energy required to establish a zero temperature difference between the sample and a reference material as each is subjected to an identical heating program it is possible to obtain the onset temperatures of hydrogen absorption/desorption. In order that the experimental procedure was carried out in an inert environment the apparatus has been installed in an argon glovebox. The onset temperatures of absorption/desorption were determined using the Netzsch Proteus software.

3.2.4 Thermo Volumetric Analysis (HTP-TPD)

An HTP volumetric analyser from Hiden was used to measure hydrogen sorption properties of the thin film samples. This volumetric apparatus records the change of the hydrogen pressure within a fixed sample volume as a result of hydrogen absorption/desorption. The samples were inertly mounted on the HTP apparatus using a special portable Ar filled glove-box. After being activated using a 100 bar hydrogen flow various isotherms were obtained as the HTP system offers fully automated operation for measuring the sample over a range of different pressures thus producing pressure composition isotherms (PCI). Moreover, the sorption kinetics of the samples were investigated using the HTP as it also provides the ability to record hydrogen uptake as a function of time. A schematic diagram of a basic Sievert –type HTP apparatus is presented in figure 3.2.

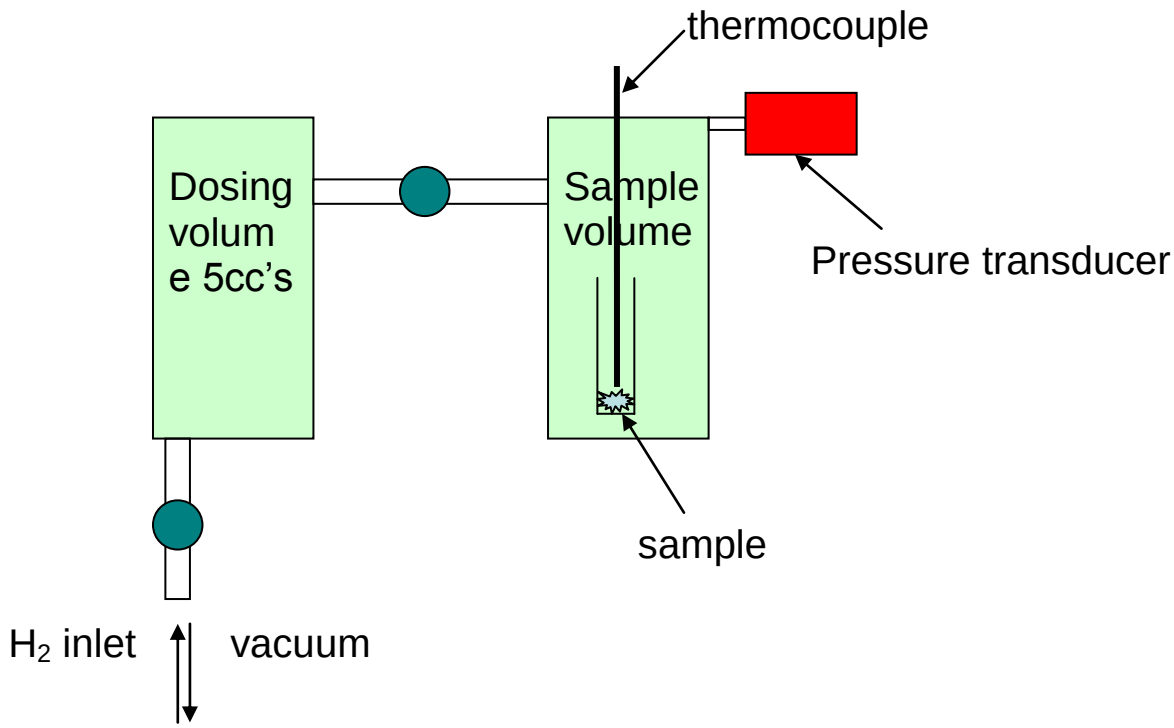

Fig. 3.2: Basic schematic of a sieverts HTP apparatus.

The HTP thermal desorption system from Hiden provides the ability to perform temperature programmed desorption (TPD) measurements. During a TPD measurement a helium carrier gas stream is applied to the sample until it reaches a certain pressure. The sample is then heated and held at a specific temperature until it stops desorbing gas species from the downstream He flow. The gas species being desorbed by the sample are detected and identified by a quadrupole mass spectrometer which is connected to the HTP apparatus. During the TPD measurement the amount of hydrogen being desorbed from the sample is plotted against the temperature increase. During both volumetric and thermal desorption measurements a portable glovebox was used to mount the samples. This was done in order to minimize oxidation of the samples.

3.2.5 Thermo Gravimetric Analysis (IGA)

Constant pressure Thermo Gravimetric Analysis, using a Hiden Intelligent Gravimetric Analyser (Hiden IGA), was carried out to determine the absorption and desoprtion of hydrogen from the samples. The IGA method involves continuously monitoring and analysing weight data following a controlled change in gas pressure. Measuring changes of the mass of the samples, allows the determination of the amount of hydrogen being absorbed. The sample is first placed on a fine microbalance which is placed inside a furnace tube. By applying a flow of hydrogen gas under controlled pressure inside the furnace tube we are able to determine the wt% of hydrogen being absorbed or desorbed from the sample. This type of analysis also provides information on kinetic parameters of absorption/desorption as it is able to record mass deviations as a function of time while setting temperatures and pressures at specific values. Finally, the IGA system can also be set to run pressure-composition isotherms. In this mode, a pressure sequence is programmed into the IGA at a

specific temperature; a kinetic trace is then recorded for each pressure step and an equilibrium absorption value is determined.

Chapter 4

Results and Discussion

4.1 Mg and Mg/Ti Thin Films

Two types of Mg/Ti thin film multilayers were successfully sputtered onto stainless steel and glass substrates. These included multilayered structures containing 8 and 14 layers, of both Mg and Ti. The largest sample was sputtered within 70 minutes and consisted of 14 layers of Mg and 14 layers of Ti, giving an overall thickness of ~7.5 μm. The average thicknesses of the Mg and Ti layers were ~440 nm and ~110 nm respectively. Given that the area of the sample was 9 cm^2, and the density of Mg is 1.74 g/cm^3, it was estimated that the total mass of Mg within this sample reached ~9.65 mg. This amount of material was not sufficient to carry out either Thermogravimetric Analysis or Thermo Volumetric Analysis using IGA or HTP respectively. These measurements would allow us to study the hydrogen storage properties of the multilayered samples. Furthermore, the dimensions of the substrates rendered the samples impractical to be mounted on the IGA and HTP apparatus. Due to this we proceeded in creating Mg/Ti multilayers with a greater amount of magnesium by increasing the number of layers. In addition to this the samples would also be deposited upon pre-cut glass substrates in order to overcome the problem of mounting the samples on the experimental equipment.

Due to various problems with the Teer Coatings magnetron sputtering system (at the University of Birmingham), it was not possible to fabricate the other samples. Therefore, Teer Coatings Ltd. produced three types of thin film samples on one of their own sputtering systems. These included:

1. Pure Mg film sample
2. Mg/Ti 20 layer thin film structure
3. Mg/Ti 40 layer thin film structure

All of the above samples were sputtered using a similar CFUBMSIP magnetron sputtering system. On the other hand, the system at Teer Coatings Ltd did not possess an embedded glove-box which would allow inert transfer of the samples.

Table 4.1: Types and characteristics of Mg and Mg/Ti thin film samples from Teer Coatings Ltd.

Sample Type	Pure Mg	Mg/Ti 20 layers	Mg/Ti 40 layers
Number of Mg layers	1	20	40
Number of Ti layers	0	21	41
Total Number of layers	1	41	81
Thickness of each Mg layer	8.8 μm	440 nm	220 nm
Thickness of each Ti layer	-	50 nm	50 nm
Total thickness	8.8 μm	9.85 μm	10.85 μm

In order to reduce oxidation, all samples were vacuum packed within 10 minutes of venting. Details of the characteristics of these thin film samples are reported in table 4.1. The aim was to attain an equal total amount of magnesium in all sample types whilst varying the number of layers. The substrates used for all sample types were sectioned glass substrates, plain glass slides, polished stainless steel squares and silicon squares. In the case of the multilayered structures, the initial and final layer sputtered during their production was titanium; this was to give rise to the cooperative phenomena through the thin film structure which would enhance the hydrogen storage properties of the samples. The values shown in table 4.1 for the thickness of the Mg and Ti layers as well as the total thickness of the samples correspond to the target values during the sputtering process. According to the SEM imaging, which is presented later on in paragraph 4.1.1, the estimated values of the thickness of the Mg layers in the 20 and 40 layer Mg/Ti structures are around 200 nm and 400 nm respectively while the Ti layers have a thickness ~70 nm. The total thickness of the pure Mg layer was estimated to be 8.75 μm while the 20 and 40 layered films showed a total thickness of ~8 μm and 10 μm respectively. In the case of the 20 layered structure the total thickness seems to be lower than expected probably due to being compressed from the Bakelite.

4.1.1 Structure of Mg and Mg/Ti thin film samples

The structures of the Mg and Mg/Ti thin films have been investigated with the use of SEM and XRD. Figure 4.1 shows scanning electron images of the cross-sections of all the thin film samples. Despite the fact that the layers of the samples are extremely thin (titanium layers in particular), the distinction between the Mg and Ti layers can be clearly observed in the SEM images. The darker areas represent the Mg layers whilst the lighter ones correspond to the Ti layers. In some cases, the upper layer of the sample was compressed by the bakelite

causing difficulties during the study of the sample, while in the case of the pure Mg film the bakelite caused detachment from the substrate. All samples were exposed to air when loaded on the microscope, however no signs of oxidation are visible from the SEM imaging.

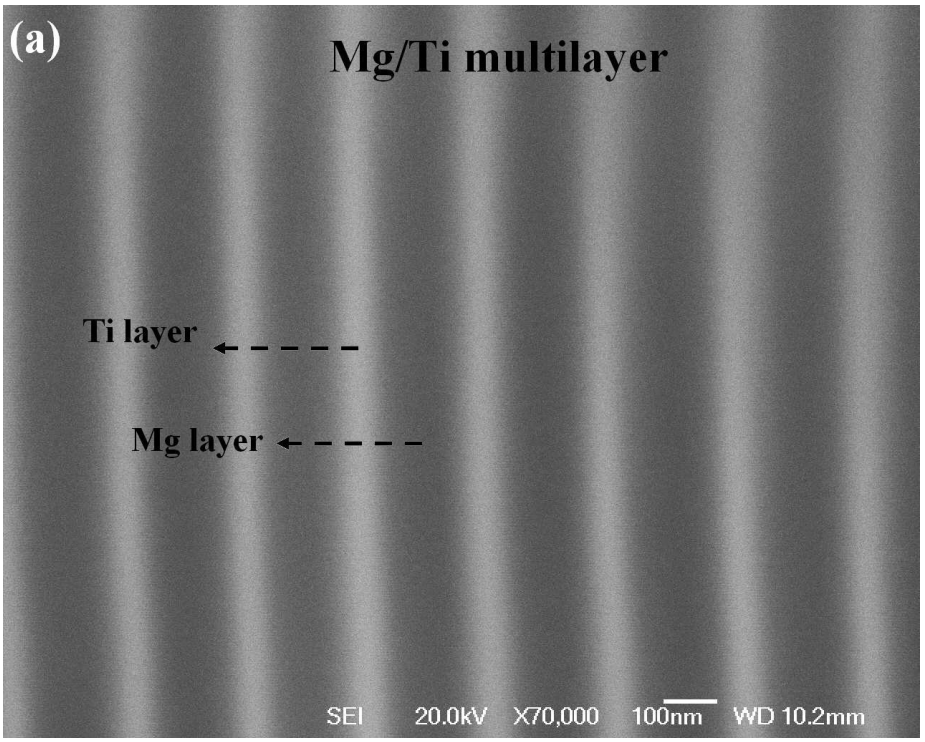

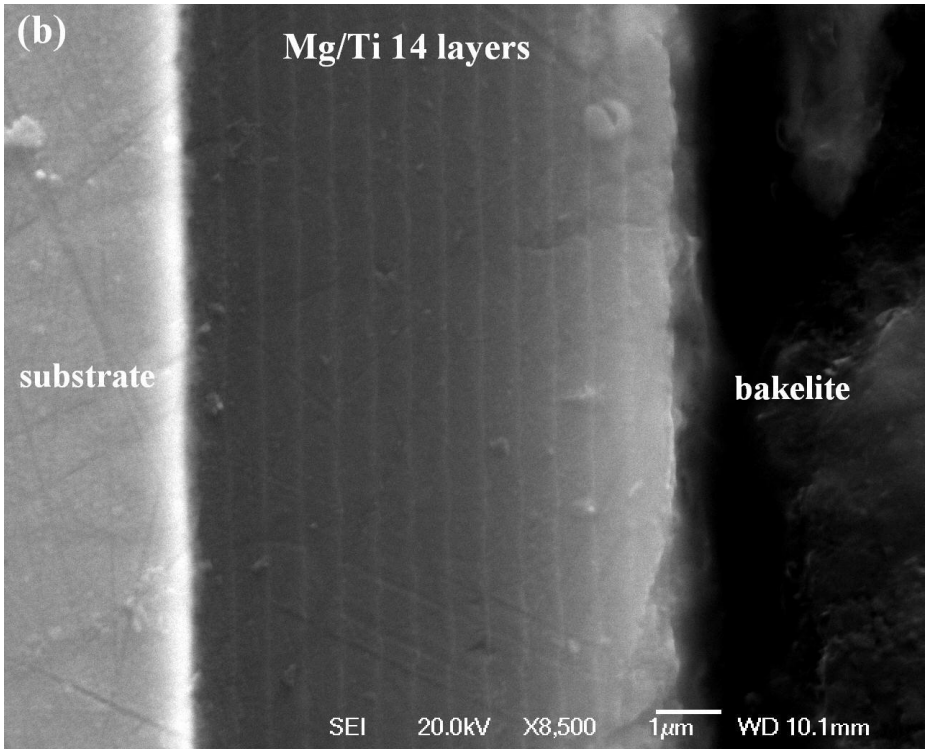

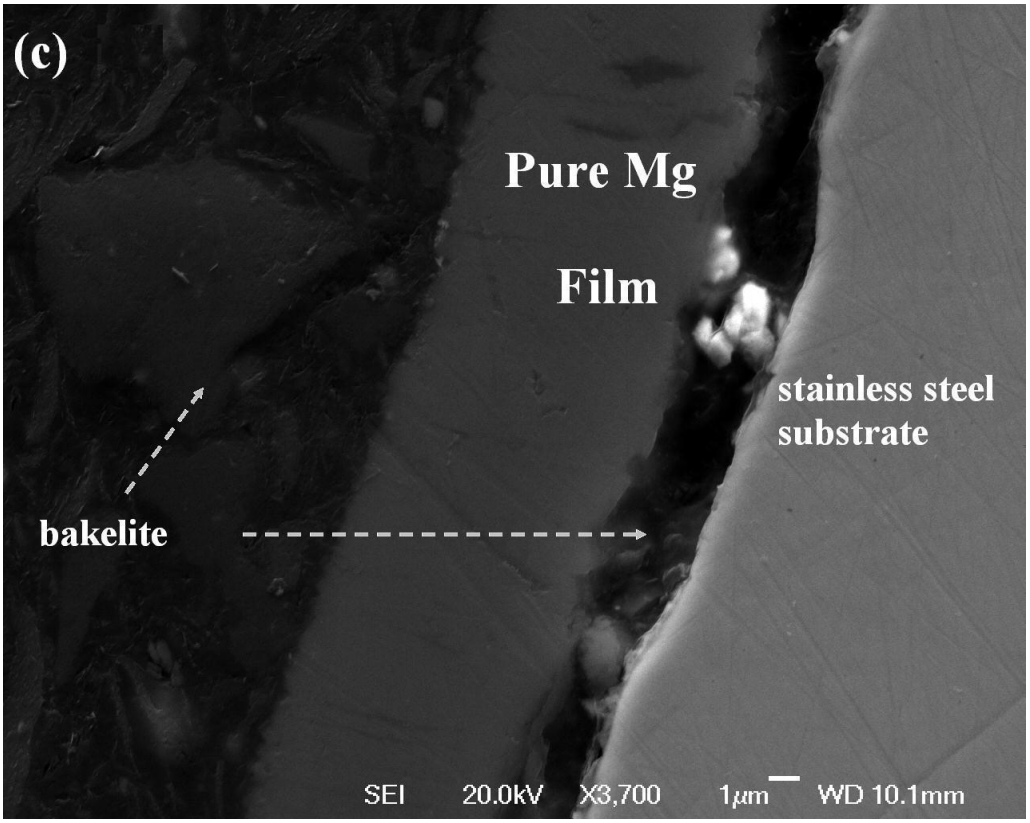
(c)
Pure Mg
Film
stainless steel
substrate
bakelite
SEI 20.0kV X3,700 1μm WD 10.1mm

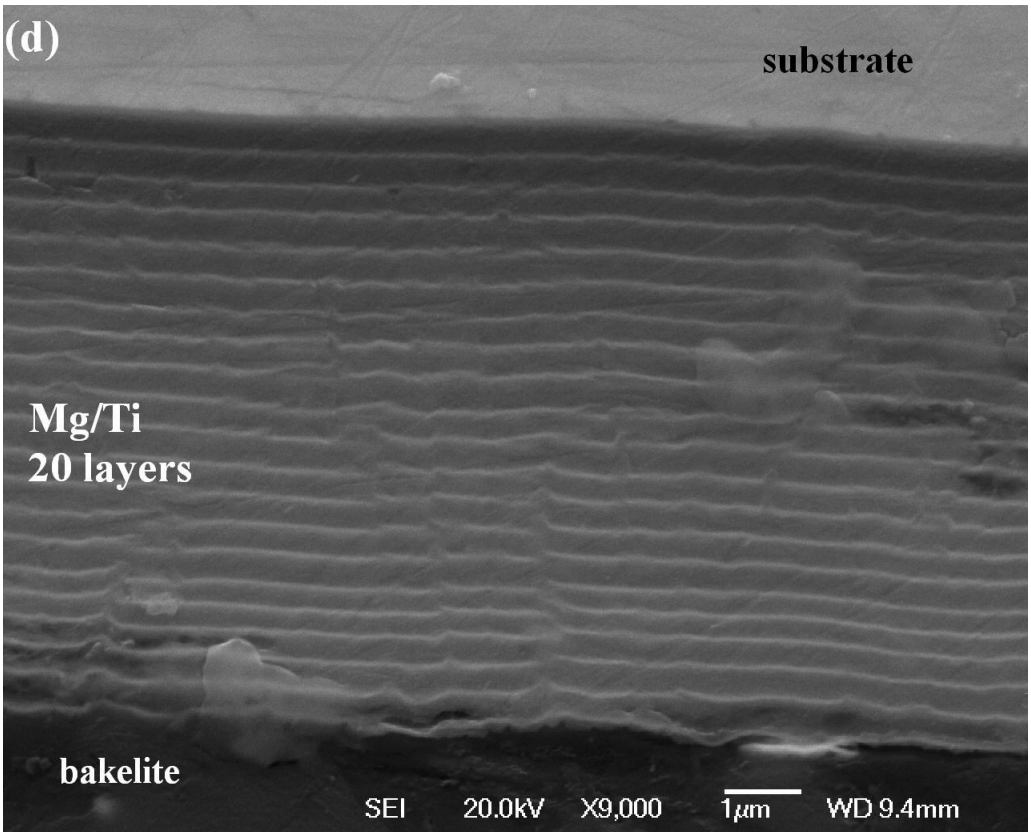
(d)
substrate
Mg/Ti
20 layers
bakelite
SEI 20.0kV X9,000 1μm WD 9.4mm

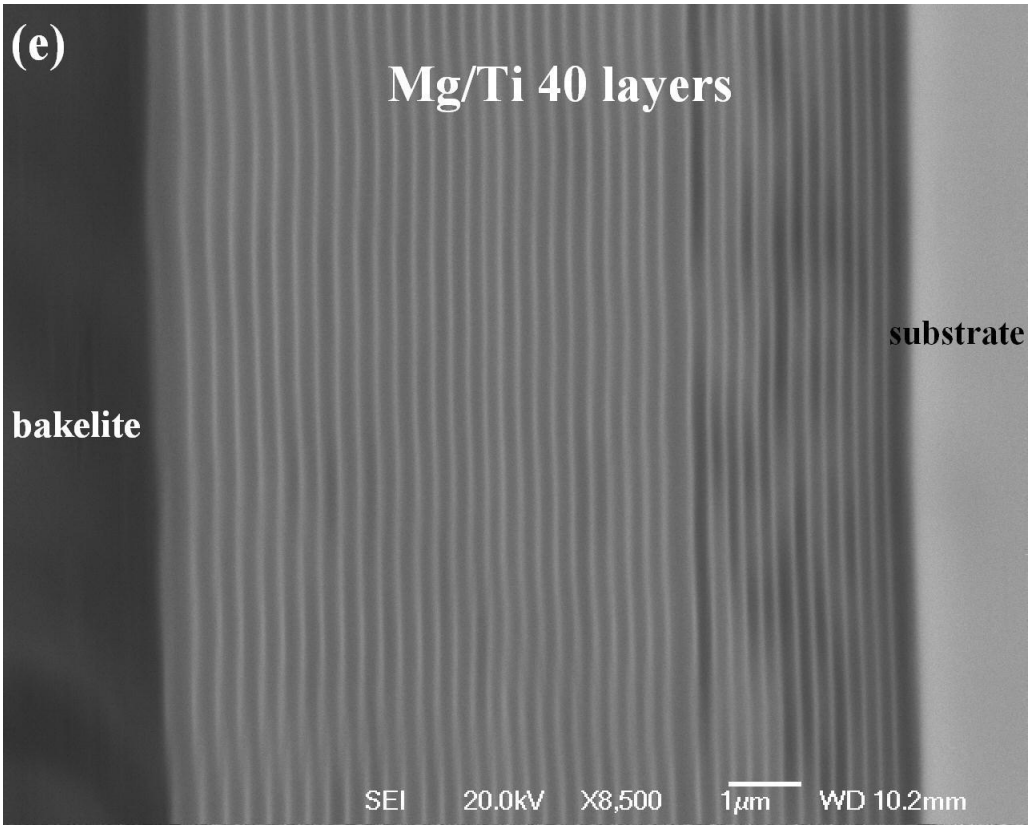

Fig. 4.1: (a) Close-up of Mg/Ti multilayer thin film sample, Scanning electron images of the cross-sections of (b) 14 layered Mg/Ti film, (c) pure Mg film, (d) 20 and (e) 40 layered Mg/Ti structures.

EDS analysis with a line spectrum was used in order to study the composition of the layers. The elements which showed the sharpest peaks were Mg and Ti while the presence of oxygen was limited to < 2 atomic%. The EDS results did not show a distinct alternation in the composition of the layers which may be attributed to the excessive thinness of the Ti layers compared to the spot size of the beam, as well as the existence of an 'intermixed' zone (co-sputtered zone of Mg and Ti) between the layers causing difficulty during the selection of the points of the line spectrum.

XRD (before hydrogenation)

The thin film samples were investigated using X-Ray diffraction prior to hydrogenation. All XRD patterns showed the presence of hexagonal Mg. Figure 4.2 shows the XRD patterns of the pure Mg film of 8.8 μm compared to Mg powder of 500 mesh size provided by Magnesium Elektron. These were taken for a 2θ range from 5-90° at room temperature.

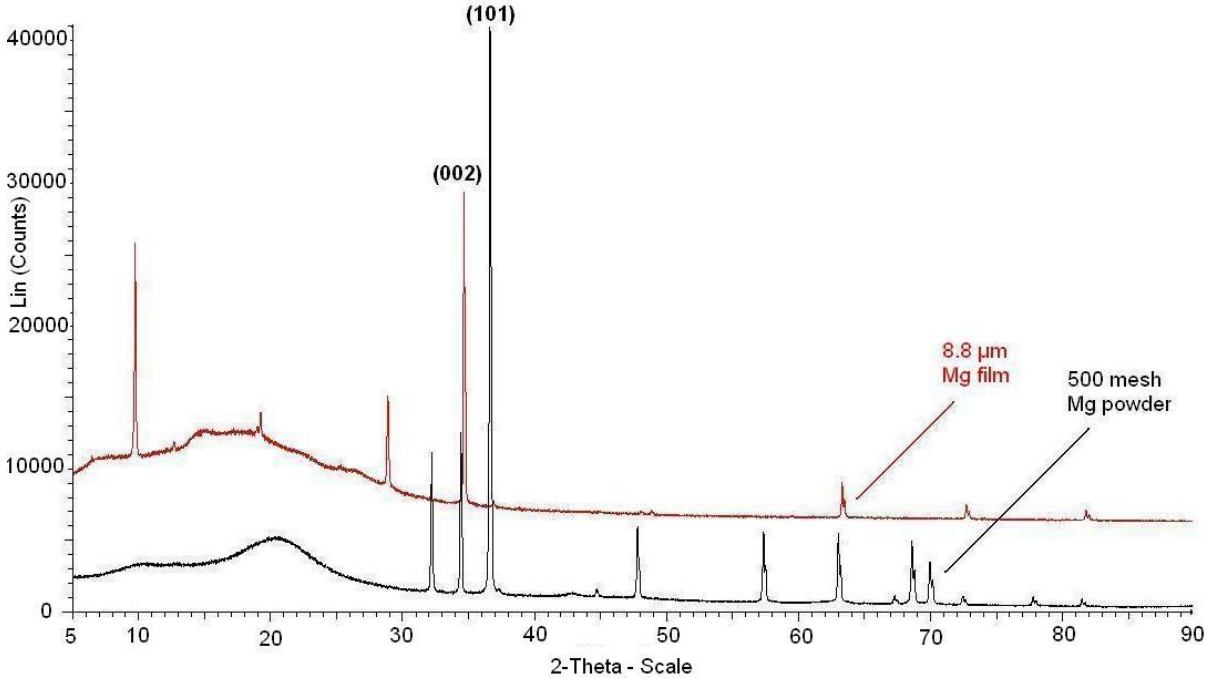

Fig. 4.2: XRD patterns of the 8.8 μm pure Mg film compared to the 500 mesh size Mg powder.

The peak with the highest intensity for the Mg film appears at about 2θ = 34.6°. This reveals the existence of crystalline Mg the growth of which is preferentially orientated along the (002) crystal plane. The Mg powder on the other hand follows the database for Mg displaying its greatest peak at a 2θ angle ~37° corresponding to the (101) plane. These results are in agreement with previous studies which have shown preferential growth of Mg films along the c-axis [26-28]. In addition, a slight XRD peak shift towards higher 2θ angles for the pure Mg film compared to the peak position of the Mg powder as well as the database

is evident in figure 4.2. This shift is induced by smaller d-spacings of the crystal structure and may be attributed to intrinsic stresses of the Mg sputtered films.

In order to avoid oxidation effects, Kapton tape and a transparent beryllium dome were used to protect the Mg film and Mg powder respectively. These inserted materials give rise to known sets of peaks which are both situated at the lower 2θ angles of the XRD scans, thus not significantly interfering with the results. Figure 4.3 illustrates the XRD pattern of the Kapton tape which is also evident in the XRD results of the Mg film.

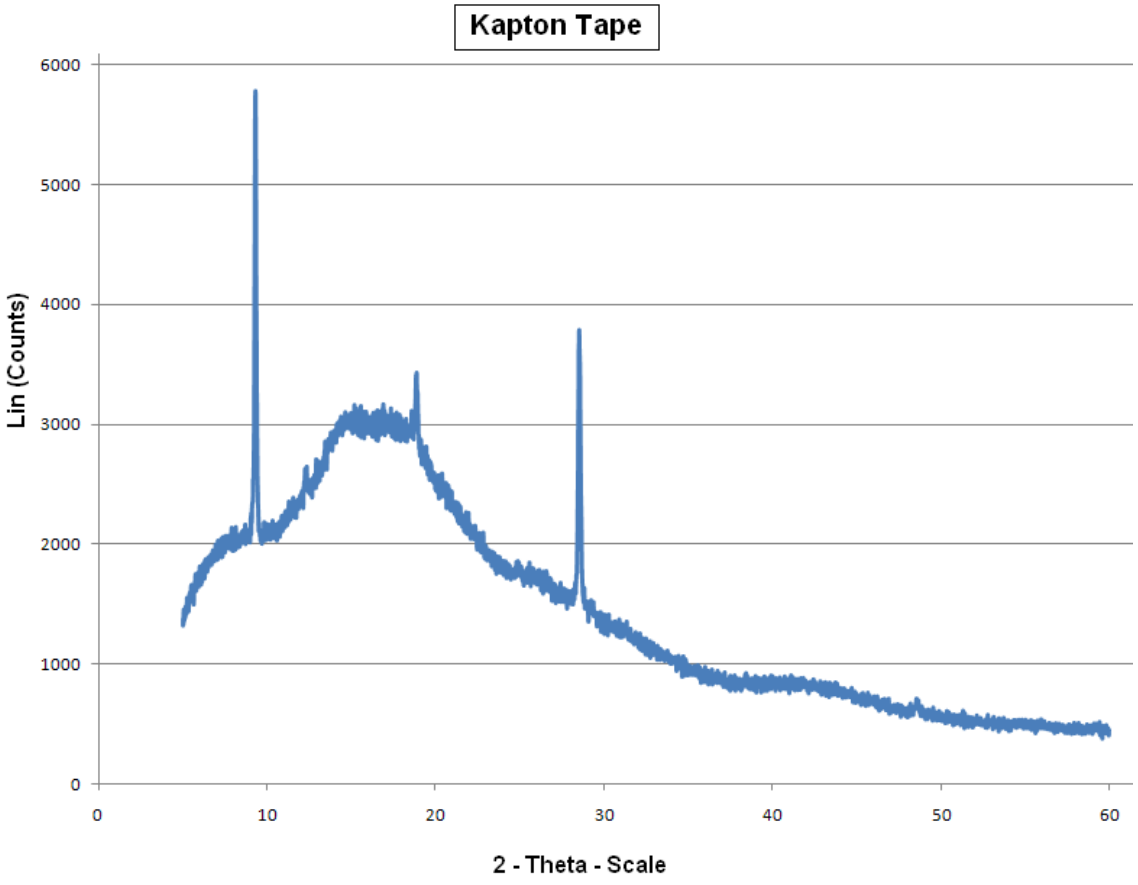

Fig. 4.3: XRD pattern of Kapton tape.

A comparison of the XRD patterns prior to hydrogenation between all multilayered samples is featured in figure 4.4. As exhibited in the case of the pure Mg film, the Mg/Ti multilayered

structures also display a preferentially orientated crystal growth along the c-axis. Again the prominent peak (~34-35°) in the XRD spectra corresponds to the (002) Mg atomic plane. Worth noticing is the difference between the visible peaks of the samples we prepared and those of the samples provided by Teer Coatings Ltd.

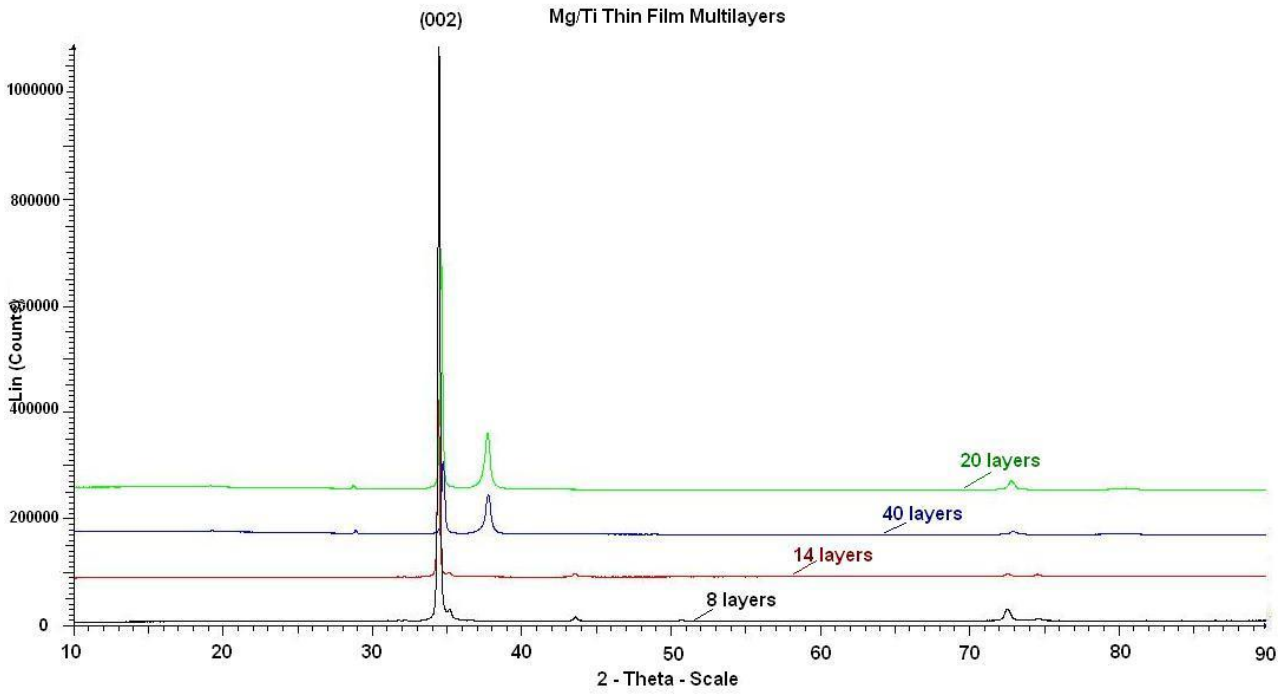

Fig. 4.4: Comparison of XRD patterns prior to hydrogenation between the 8 and 14 layered structures produced at the University of Birmingham as well as the 20 and 40 Mg/Ti multilayered samples from Teer Coatings.

The black and red lines represent the 8 and 14 layered Mg/Ti samples respectively and display a small peak beside the Mg (002) major peak at ~35.2° which is ascribed to titanium. This peak is not visible in the cases of the 20 (green line) and 40 (blue line) layered structures (from Teer Coatings) while contrary to the 8 and 14 layered samples (from the University of Birmingham), these display a significantly sharp peak at around 37.5°. The last peak is quite broad while having a slight asymmetric shape probably due to a combination of Mg and Ti peaks and induced lattice strains [22]. The observed differences between the XRD

patterns and therefore the crystallization of the samples we prepared and those stemming from the Teer Coatings samples may be ascribed to variations in the sputtering conditions [53]. Again a slight peak shift towards higher 2θ angles is evident for the peak positions of the Mg/Ti multilayers from Teer Coatings compared to peaks reported from the database. This shows that the spacing between the lattice planes has decreased due to intrinsic stresses within these thin film samples. Stresses present in the thin films could be relieved by heating the sample, whereas in situ XRD measurements at different temperatures could be used to investigate the samples.

On the other hand, a possible cause of the observed peak-shift towards higher angles might be attributed to material substitution at the Mg/Ti interfaces. The interpolated Ti atoms within the Mg metal structure may also contraction of the lattice, thus inducing a 2θ shift towards higher angles (smaller d-spacings). The contraction of the metal lattice is due to the smaller molar volume of Ti compared to Mg. This result is in agreement with results from Vermeulen et al. where the increasing partial substitution shows a transition towards larger angles of the XRD peaks [43]. The existence of intermixing zones may give rise to a Mg-Ti single phase fcc-structured hydride, upon hydrogenation which may improve hydrogen insertion compared to the common bct structure of MgH_2 [43,44].

4.1.2 Hydrogenation of Mg and Mg/Ti thin film samples

4.1.2.1 HTP measurements on Mg and Mg/Ti thin films

An HTP experimental apparatus from Hiden was used to carry out volumetric analysis and therefore assess the hydrogen sorption properties of the thin film structures. At first, five pure Mg films deposited on pre-cut glass strips were mounted on the HTP device. Each glass

strip had dimensions of ~0.4 x 2.6 cm; this in combination with the density of Mg being 1.74 g/cm^3 and the 8.8 μm thickness of the film, gives a ~1.6 mg mass of Mg. The total mass of all 5 slides used for the HTP measurements reaches almost 8 mg. The mass of Mg deposited upon a thin film strip with the above dimensions is the same for all thin film samples while the total mass of each sample varies depending on the number of Ti layers.

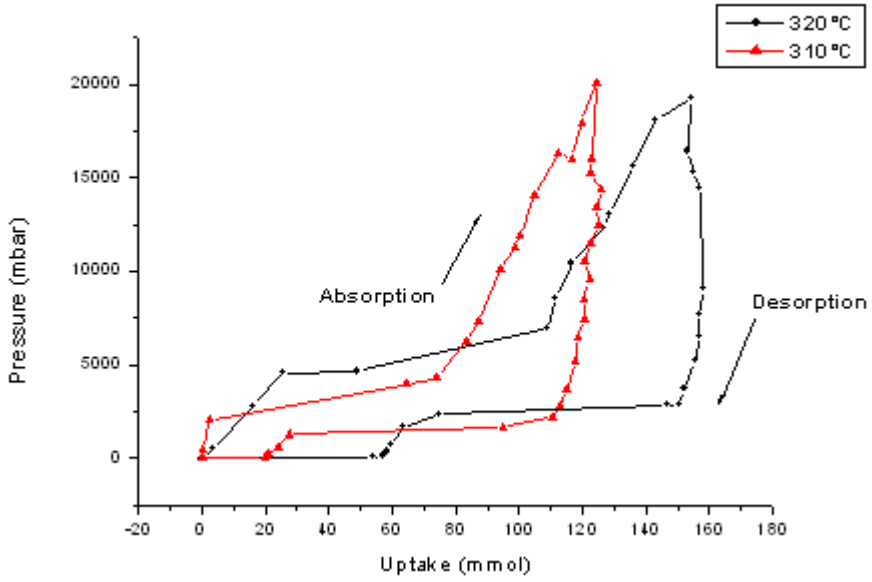

Fig. 4.5: PCI diagrams of absorption and desorption of the pure Mg film at 310 and 320°C.

As mentioned in Chapter 2, the target Mg sample mass is kept constant, while the number of layers is altered. The pure Mg sample was inertly mounted on the HTP apparatus using a special portable Ar glove-box. Once the sample was loaded, a 100 bar hydrogen flow was used to activate the sample at 320°C. One of the glass slides was then removed from the sample holder and examined using XRD to investigate the presence of any hydride phase(s). The remaining 4 slides with Mg were used for obtaining pressure concentration isotherms (PCI) at 310 and 320°C using the HTP apparatus.

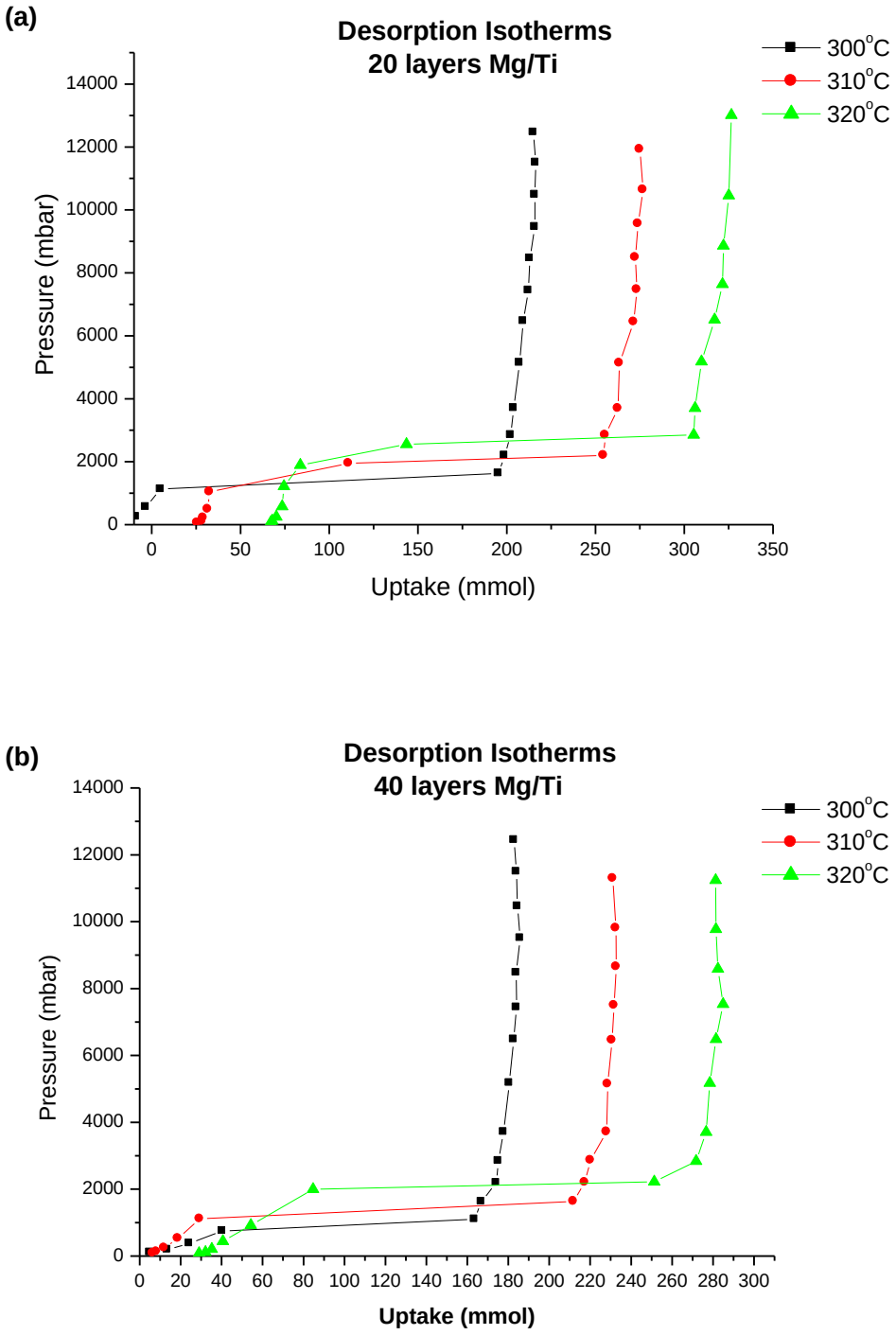

Fig. 4.6: Desorption isotherms of the (a) 20 and (b) 40 layered Mg/Ti thin film samples.

The PCI diagrams of pure Mg are presented in figure 4.5. The points at which the pressure steps abnormally deviated during the measurements (due to problems with the HTP

software) were removed in order to give a clearer image of the isotherms. The plateau during hydrogen absorption presents a slope, while the plateau of desorption is almost parallel to the x-axis. The slope in the absorption plateau makes the accurate determination of the plateau pressure quite difficult. The same experimental procedure was carried out for the Mg/Ti 20 and 40 multilayered samples. For the latter samples, apart from the isotherms at 310 and 320°C an additional one at 300°C was obtained.

Only the desorption isotherms of the 20 and 40 layered Mg/Ti thin film samples are presented in figure 4.6 as once again the absorption plateaus are inclined. The PCI diagrams of all the samples display an offset between the isotherms due to a small leak in the HTP system.

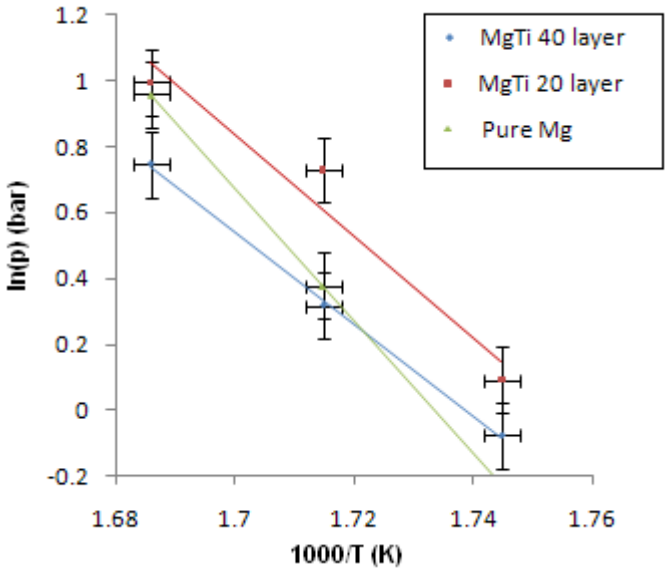

Fig. 4.7: Van't Hoff plots and error bars of hydrogen desorption for the pure Mg as well as the 20 and 40 layered Mg/Ti films.

The logarithmic value of the pressure at the middle point of the PCI plateaus plotted against the temperature inverse gives a van't Hoff plot. These linear plots and error analysis for

hydrogen desorption of all three samples are presented in figure 4.7. The error for the HTP apparatus was +/- 1°C and +/- 0.1 bar giving rise to significantly large error bars. As mentioned earlier in Chapter 1, the van't Hoff plot allows the determination of changes in thermodynamic properties of materials. From the slopes of the van't Hoff plots it is possible to calculate the desorption enthalpies of the samples. For the pure Mg sample the enthalpy was estimated to be around -167 kJ/mol, while the values for the 20 and 40 layered samples were -128 kJ/mol and -116 kJ/mol respectively. These values are quite high compared to the average value of formation and decomposition of MgH_2 arising from the literature which is around -75 kJ/mol [14]. On the other hand, it is worth noting the difference between the enthalpies of the samples with the highest enthalpy corresponding to the pure Mg sample. The second largest value corresponds to the 20 layered sample while the 40 layered sample displays the smallest enthalpy. Due to the large errors these results are not so reliable. According to linear fittings of our results, the Mg/Ti films are able to desorb at lower temperatures compared to pure Mg, meanwhile the sample with the greater number of layers might exhibit an even lower temperature of desorption compared to the sample with less layers. These results can be attributed to the increased influence of the cooperative phenomena with increasing the number of layers within the multilayer structure. Moreover, the lower desorption temperature of the multilayered samples compared to the pure Mg sample might be due to a metastable state at the Mg/Ti interfaces (type of alloying at 'intermixed' areas) as Vermeulen et al. have reported for Mg-Ti thin films [43].

4.1.2.2 XRD measurements on hydrided Mg and Mg/Ti thin films

As mentioned above, one glass slide of each sample was removed from the HTP after the hydrogen storage material was activated. XRD measurements were carried out on each sample to investigate the presence of hydrided phases. Kapton tape was put over the sample in order to minimize effects of oxidation. All the XRD measurements were taken with a 2θ range from 5-90° at room temperature.

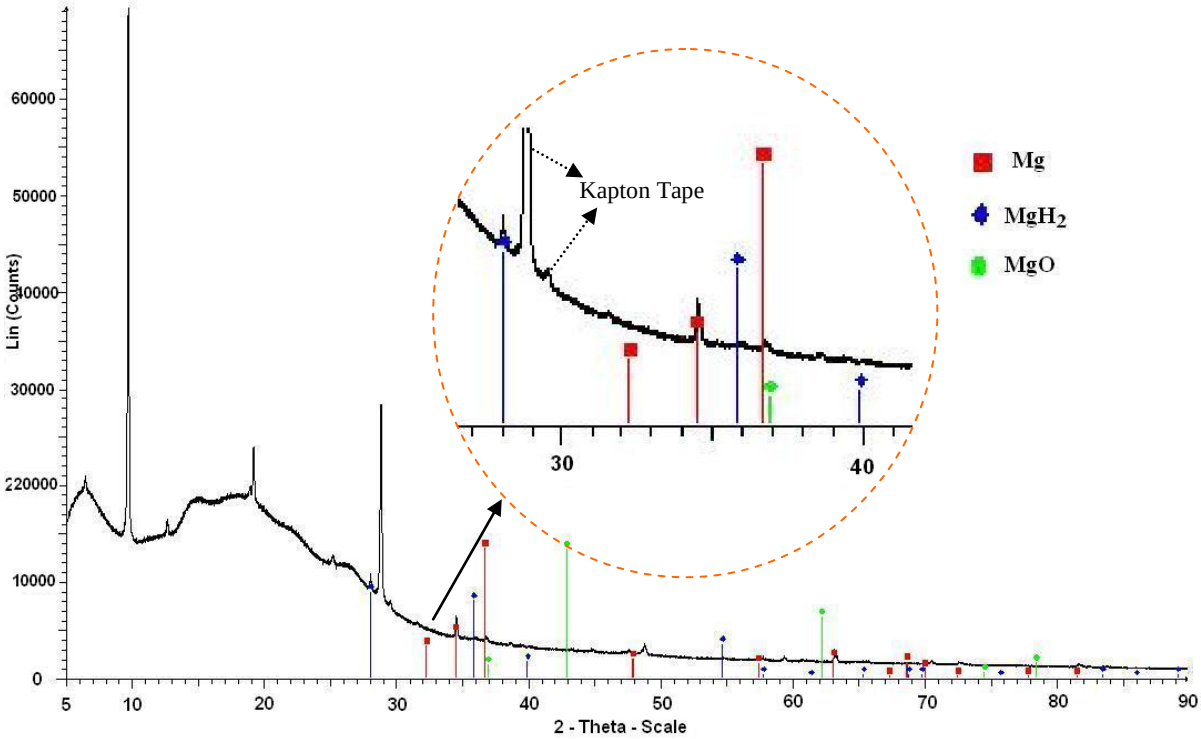

Fig. 4.8: XRD spectrum after hydrogenation of the pure Mg film.

The XRD spectrum following hydrogenation of the pure Mg sample is presented above in figure 4.8. As we can see the Mg peaks in the XRD pattern almost disappear compared those of the pre-hydrogenated samples, while a peak at 28° is attributed to MgH_2 confirming that the absorption of hydrogen occurred within the pure magnesium film.

It is difficult to distinguish the MgH_2 peak as it is positioned within the peak area of the Kapton tape*. Another quite small MgH_2 peak is positioned at 35.9°. It is worth noting that all peaks are quite weak most probably due to the presence of the protective Kapton tape.

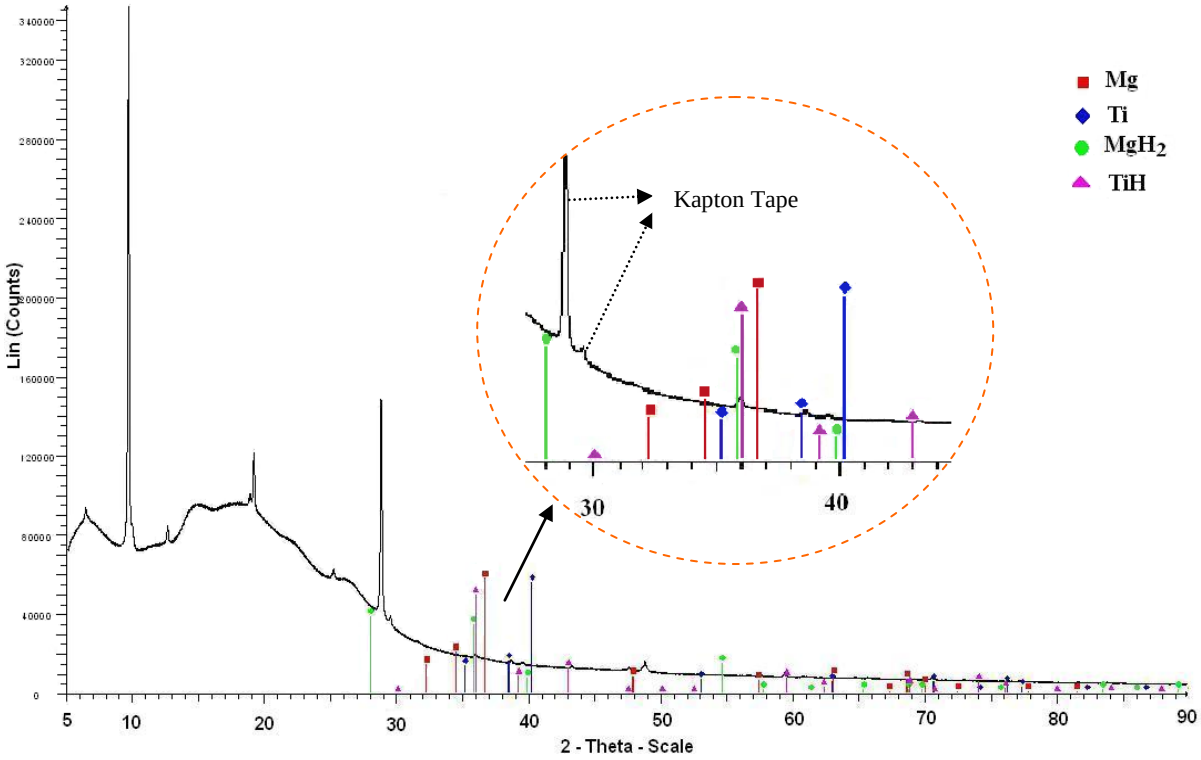

Fig. 4.9: XRD spectrum after hydrogenation of the 20 layered Mg/Ti thin film sample.

** For reasons of clarity all peaks due to the Kapton tape (figure 4.3) are not presented in the XRD results. It is worth noting that the broad prospective peak due to the glass substrates near the range 20-30° is also within the 2θ range of the Kapton tape and is not indexed in the XRD results [45].*

Figure 4.9 shows the XRD pattern for the 20 layered Mg/Ti sample. The intensities of the Mg and Ti peaks have dropped, while the most intense Mg peak at 34-35° displays a strong broadening due to a combination of various peaks. A quite strong MgH_2 peak appears at 35.9° just like the case of the pure Mg sample. Some TiH significantly small peaks can barely be distinguished within the XRD spectrum due to the presence of the Kapton tape.

The XRD pattern of the 40 layered Mg/Ti sample (figure 4.10) once again shows a significant MgH_2 peak at 35.9° and only a few peaks of hydrided phases which are not clearly evident due to the Kapton tape (figure 4.3).

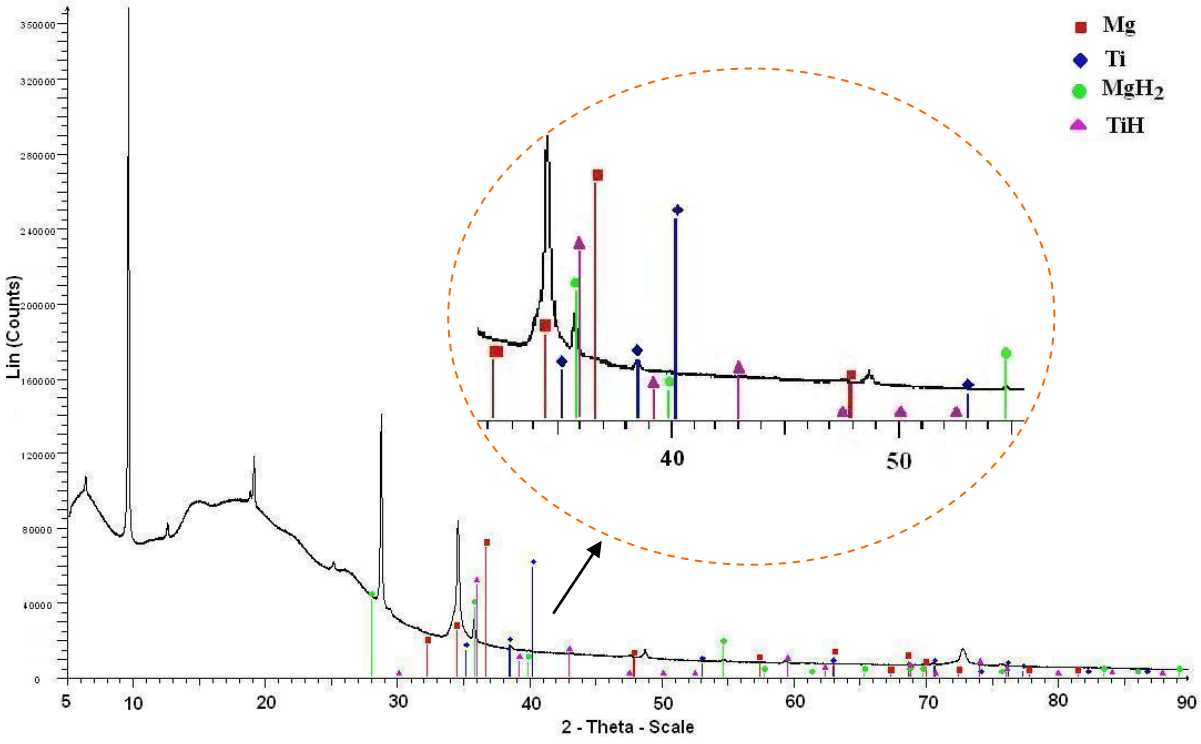

Fig. 4.10: XRD pattern after hydrogenation of the 40 layered Mg/Ti thin film sample.

4.1.2.3 TPD measurements on Mg and Mg/Ti thin films

After obtaining pressure-concentration-isotherms, the HTP apparatus was programmed to carry out temperature programmed desorption (TPD) measurements of all the hydrided

samples, while connected to a mass spectrometer. The temperature range during the TPD measurements was 205-450°C with a 10 K/min heating rate, while the He flow reached 100 ml/min. The mass spectrometer used by the TPD was uncalibrated meaning that a quantitative determination of the desorbed gases from the resulting data was not possible. However, the error that appears in the measurements is consistent and therefore the results on the samples are directly comparable. Figure 4.11 presents the TPD results of all three sample types. It is clear that both Mg/Ti multilayered samples desorb a significant amount of hydrogen at quite an early stage (320-360°C) compared to the pure Mg sample. The samples present an onset temperature of hydrogen desorption around 315-320°C.

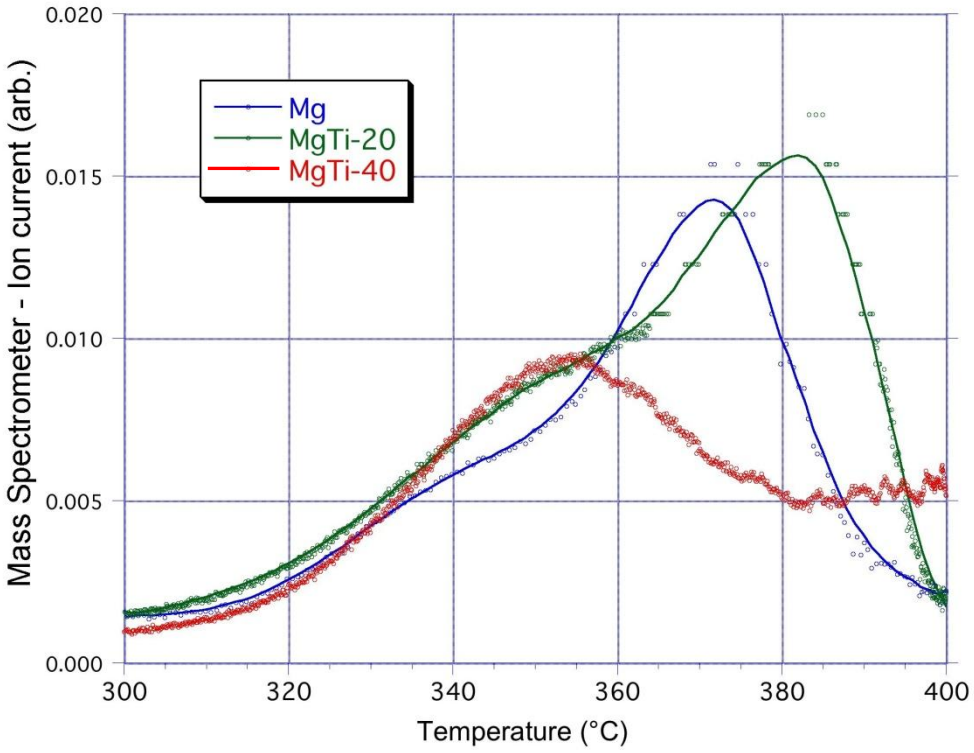

Fig. 4.11: TPD results of the pure Mg film and 20 and 40 layered Mg/Ti multilayered samples.

The intrinsic pressures developed within the thin film multilayer samples due the cooperative phenomena are responsible for lowering the temperature of hydrogen desorption [45,46]. Because the larger number of layers and therefore greater induced pressures within the

sample, the 40 layered structure was expected to exhibit the lowest desorption temperature of all three samples, however the TPD results did not show any significant difference between the desorption temperatures of all three samples. The pure Mg as well as the 20 layered Mg/Ti sample appear to desorb hydrogen in two steps displaying a 'shoulder' in their TPD diagrams in figure 4.11. This might be attributed to the existence of a high pressure γ-phase of magnesium hydride which is metastable and may initially desorb a sufficient amount of hydrogen at lower temperatures than the common β-MgH_2 phase. In the case of the 40 layered Mg/Ti sample, the TPD graph displays a smaller and symmetric peak of hydrogen desorption compared to those of the other two samples. It is possible that the desorption process for the 40 layered sample was not completed as the ion current does not approach zero as displayed for the other two samples.

After removing the 40 layered sample from the HTP apparatus after the TPD measurements we observed bubbles on the surface of the sample (figure 4.12). This was due to trapped hydrogen within the sample which was not able to surpass the outer layer (or layers) of the Mg/Ti structure during the desorption process.

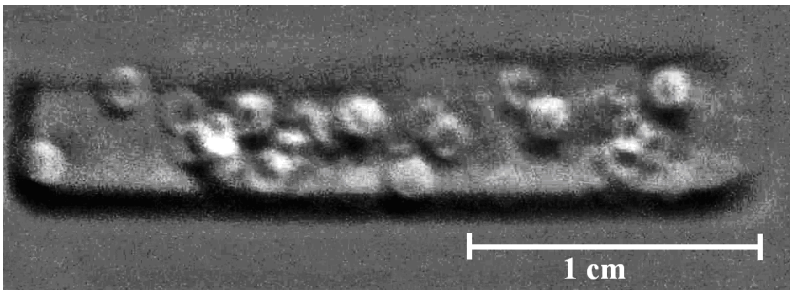

Fig. 4.12: Photograph of the 40 layered sample after the TPD measurements. Bubbles can be clearly observed on the sample surface.

In the case of detachment of the layers within the structure the cooperative phenomena would not be able to fully take place as the induced stresses are relieved.

4.1.2.4 Kinetic Points using the HTP on Mg and Mg/Ti thin films

In order to investigate the hydrogen sorption kinetics of the samples, the HTP was used to carry out hydrogen absorption and desorption measurements whilst maintaining the same experimental conditions. During both absorption and desorption measurements, the temperature was kept at 320°C while the pressure was 20 bar and under 1 bar for hydrogen absorption and desorption respectively. The hydrogen uptake plotted against time is presented in figure 4.13. These plots when set on the same x-axis could not give a clear image of the sorption kinetics.

During hydrogen absorption the 40 layered sample exhibited faster kinetics than the pure Mg and 20 layered Mg/Ti samples. From the plots below it is clear that the 40 layered sample presents the steepest curve and therefore a rapid hydrogen uptake. This was expected due to the contribution of the greater number of layers to the cooperative phenomenon as discussed in paragraph 2.5 [45,46]. On the other hand, the 20 layered sample did not show a great amount of hydrogen uptake, although it reached its highest point quite fast. Finally, the pure Mg sample displayed the slowest kinetics of all samples just as expected as it did not contain a catalytic material, which according to literature would accelerate hydrogen desorption upon the Mg surface, or have a performance enhancing structure which apart from lowering the desorption temperature has been proven to boost the sorption kinetics of Mg [30-36,45].

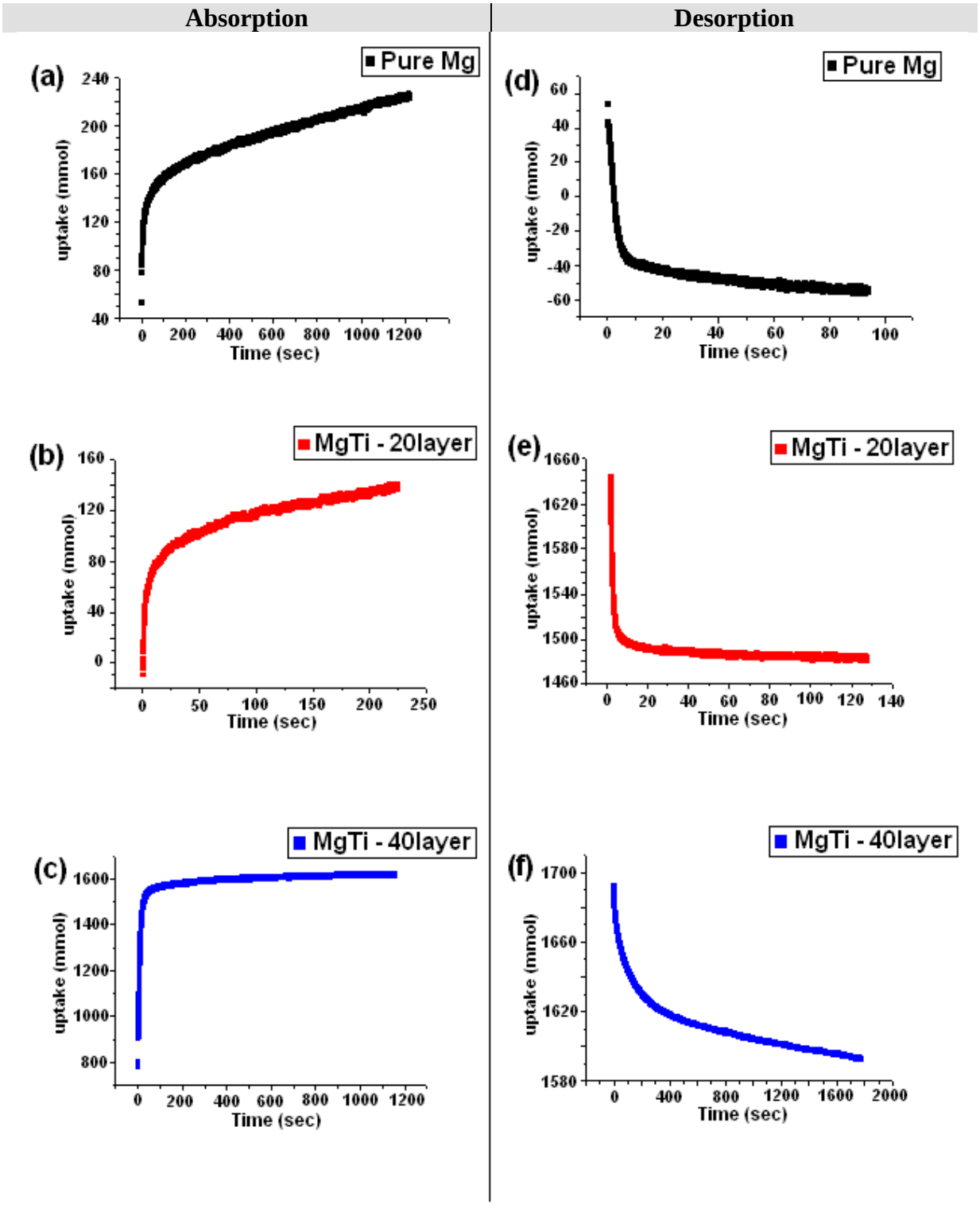

Fig. 4.13: Hydrogen uptake versus time for absorption/desorption: (a)-(d) pure Mg, (b)-(e) 20 layered and (c)-(f) 40 layered Mg/Ti structures.

During hydrogen desorption, the 40 layered sample displayed the slowest kinetics of all samples unlike the case during hydrogen absorption and contrary to what we expected. On the other hand the 20 layered and the pure Mg samples presented similar performance, both desorbing a great amount of hydrogen at an early stage. The 20 layered structure exhibited the most rapid kinetics of all three samples due to the influence of the cooperative phenomena. Future work could focus on the comparison of the hydrogen sorption kinetics of Mg/Ti multilayered samples with other nano and constrained hydrogen storage systems under the same experimental conditions.

4.1.2.5 Final XRD measurements on Mg thin films

XRD measurements were also performed on each sample for a 2θ range from 5-90° at room temperature after they were dismounted off the HTP system. This was to investigate the presence of remaining hydrided phases within the samples after their dehydrogenation using the HTP. Once again Kapton tape (figure 4.3) was used to protect the samples from oxidising, therefore having a negative effect on the peak intensities of the XRD patterns.

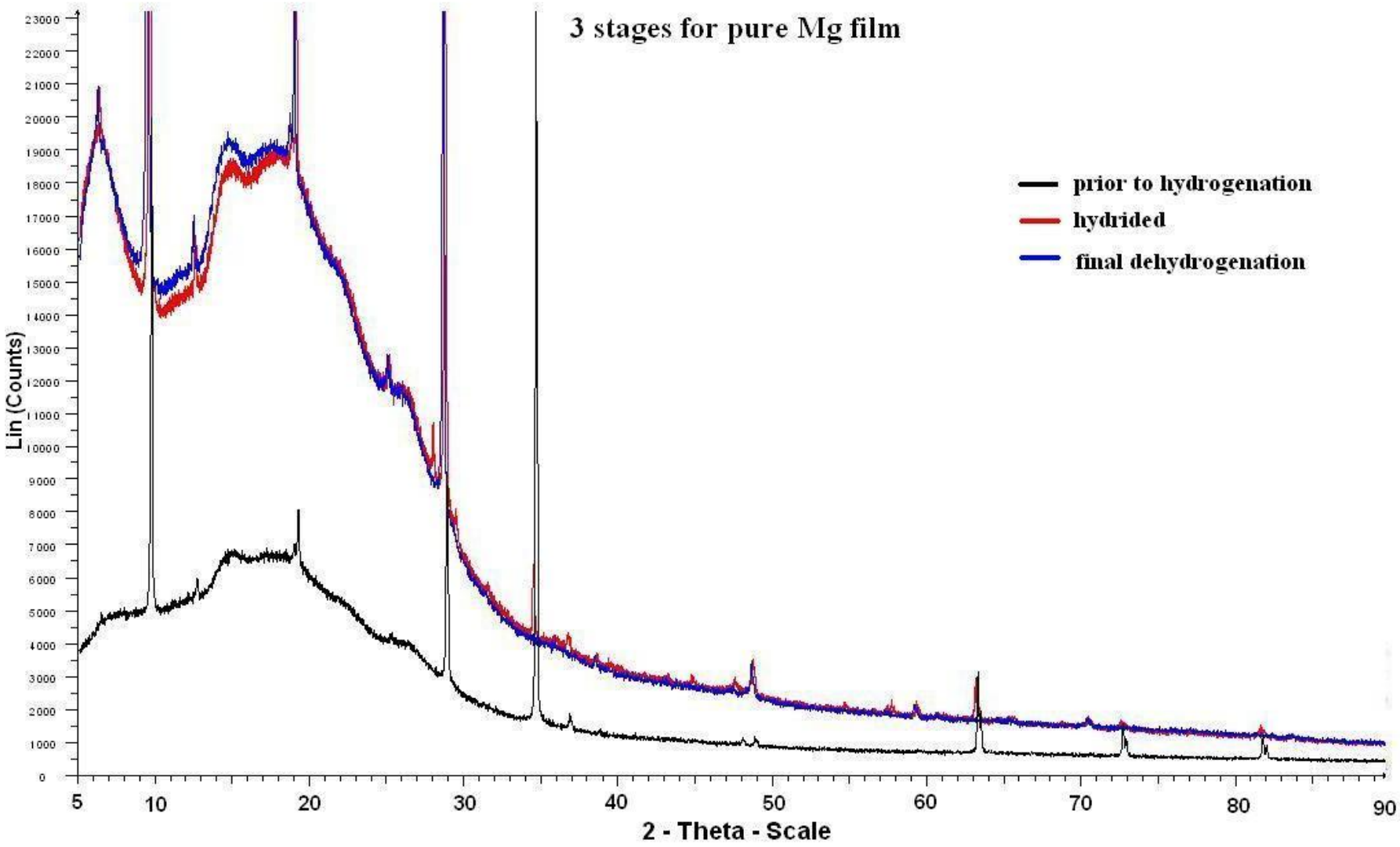

Fig. 4.14: Comparison of the XRD spectra of pure Mg prior to hydrogenation, after being hydrided and finally being dehydrogenated.

Figure 4.14 displays a comparison of the XRD spectra of pure Mg prior to hydrogenation, after being hydrided and finally being dehydrogenated. The MgH_2 peak at 28° disappears after hydrogen has been desorbed while the Mg peak around 34-35°, which was prominent in the pre-hydrogenated pattern and lowered in the hydrided sample, is not visible after dehydrogenation due to the Kapton tape.

The XRD results of the 20 layered Mg/Ti sample after it was removed from the HTP apparatus showed very few peaks of imperceptible intensity do the Kapton tape. The Mg peak at 34-35° displays an asymmetric broadening due to the existence of an adjacent Ti peak.

The 40 layered thin film structure displays the formation of a broad ‘shoulder’ peak right next to the Mg prominent peak (34-35°). This appears to be the approaching of the 34.5° and 35.9° peaks presented in the results of the hydrided sample (figure 4.15). Most likely the 40 layered sample was not completely dehydrogenated after the HTP measurements. This is in agreement with the results on TPD measurements.

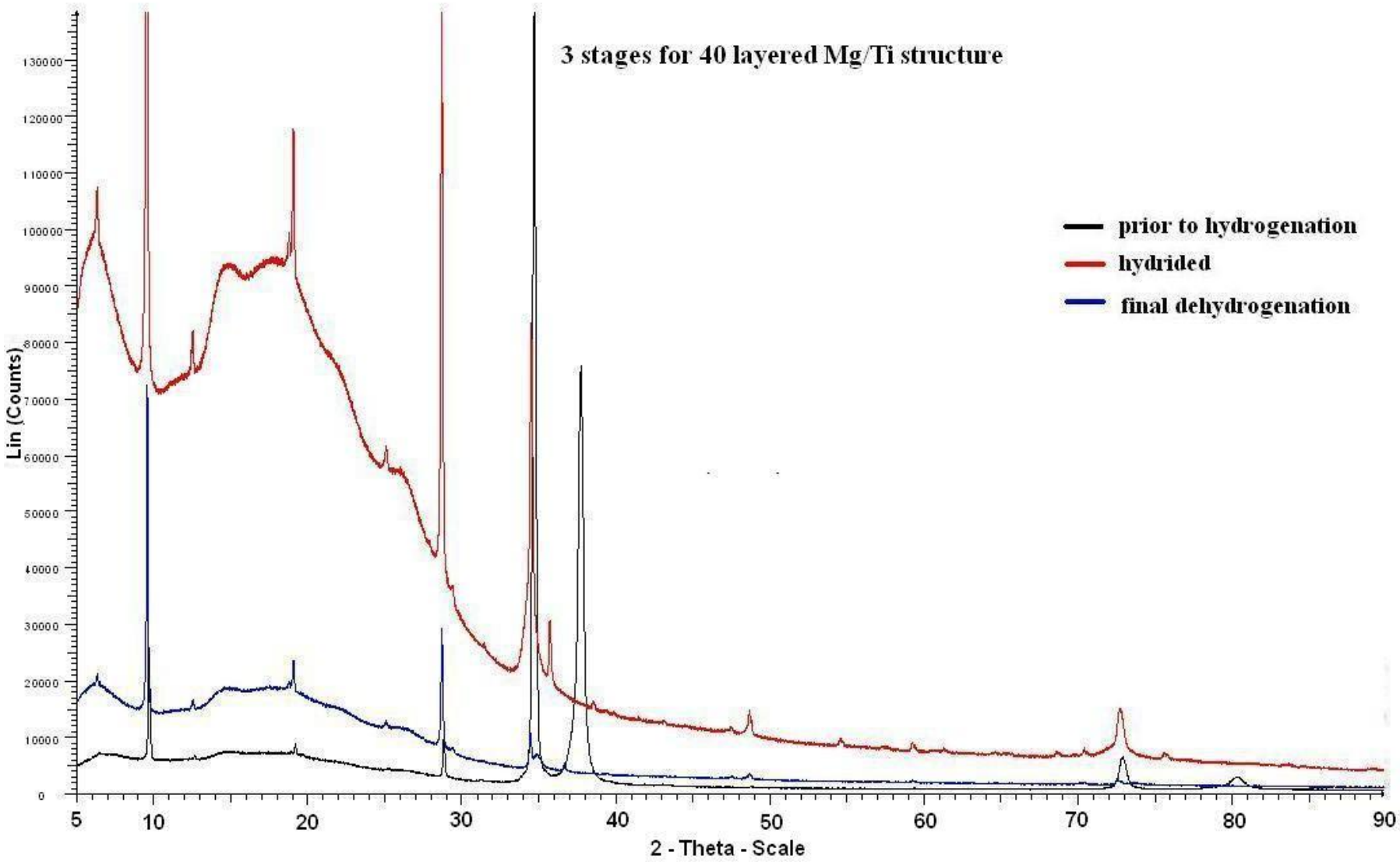

Fig. 4.15: Comparison of the XRD spectra of the 40 layered Mg/Ti sample prior to hydrogenation, after being hydrided and finally being dehydrogenated.

To sum up the XRD results on the thin film samples, apart from the disappearance of the MgH_2 peak at 28° for the pure Mg sample, do not show a clear dehydrogenation and magnification of the prominent Mg peaks. According to literature we expected the peaks corresponding to Mg reflections to reappear after dehydrogenation and the initial structure of the film to be restored thus proving cyclability of the structures [26-27]. This was not observed most likely due to the effect of the kapton tape, while in the case of the 40 layered structure the sample did not show signs of dehydrogenation but the persistence of hydrided peaks. For the latter, the induced stresses seemed to be relieved after detachment of the layers within the structure thus hindering hydrogen desorption. This is in agreement with Fujii et al who reported detachment and unfavourable hydrogen sorption characteristics for samples with greater Mg thickness [45].

4.1.2.6 IGA measurements on Mg and Mg/Ti thin films

An attempt to determine the amount of hydrogen being absorbed and later desorbed by the thin film samples was carried out by constant-pressure Thermogravimetric Analysis, using a Hiden Intelligent Gravimetric Analyser (IGA). At first, the pure Mg film deposited upon a glass slide was carefully cut inside an argon glove-box using a glass cutter. The cut samples were then mounted in an improvised sample container fabricated using stainless steel film (figure 4.16).

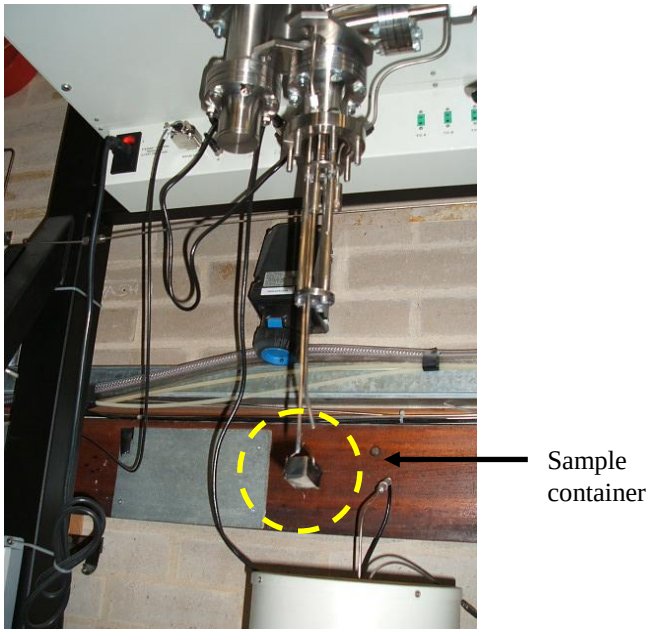

Fig. 4.16: Image of the sample container mounted upon the Hiden IGA experimental apparatus.

The total mass of the sample (~ 4g) plus the sample holder (~1g) had to be under 5g. The large mass of the sample does not allow a typical measurement using the IGA. Once the sample was mounted, the system was outgassed at 10^{-6} mbar using a turbomolecular pump supported by a diaphragm pump. The sample was then heated up to 340°C in 18 bar H_2, once the temperature was stable the IGA was run for 1000 min recording the mass, pressure and temperature against time. Unfortunately, no mass of hydrogen uptake was observed during these measurements. This is attributed to the lack of sensitivity of the IGA balance even with such an amount of sample proving this method difficult for measuring hydrogen storage properties of Mg films.

4.2 Magnesium Powders

An alternative way to try to achieve improved hydrogen sorption properties in magnesium is through the fabrication of Mg powders, with increased specific surface area. As mentioned in Chapter 3, magnesium nano-powders (<100 nm) were provided by Dr Isaac Chang (School of Metallurgy and Materials) and Metal Nanopowders Ltd. In addition to this, gas atomised Mg powder of 500 mesh supplied by Magnesium Elektron, Mg powder from Alpha Aesar of -325 mesh and MgH_2 of 325 mesh obtained from Goldschmidt were used to investigate the correlation between the particle size of Mg powders and their hydrogen sorption characteristics.

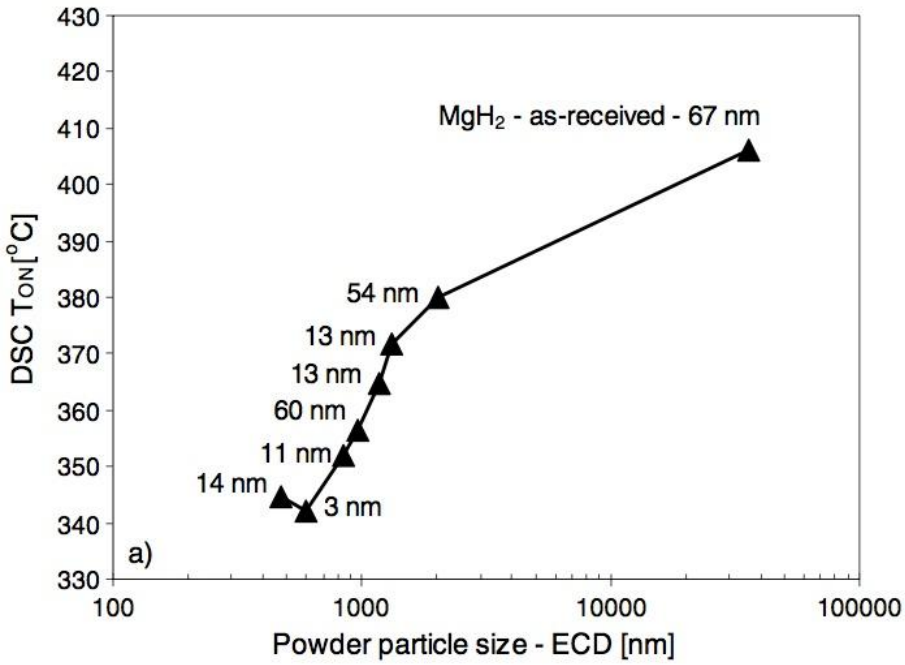

Fig. 4.17: DSC onset temperatures versus particle size.

As discussed earlier in Chapter 2 by increasing the particle size of Mg it is possible to achieve a lower temperature of hydrogen desorption. Figure 4.17 shows this correlation between the particle size and DSC onset temperatures of desorption for MgH_2 [22].

The grain size of the Mg powder is another important characteristic that positively affects the performance of Mg powders as the lower packing density of the metal atoms enhancing hydrogen diffusion [16]. In this study the determination of the grain size was not feasible; although this was attempted by etching the powders which were first mounted into conducting bakelite and then investigated using a confocal microscope.

4.2.1 DSC measurements on Mg powders

DSC was also performed on all magnesium powdered samples recording the heat flow as a function of temperature. At first, each sample was heated from 30 to 500°C and then cooled backed down to 30°C. The heating rate was at 5°C/min while the sample was under 25 bar of hydrogen. The same procedure was carried out for a variety of different pressures of H_2 (3, 10, 15, 20 and 25 bar). Figure 4.18 displays the results of the DSC measurements of the Mg -325 mesh powdered sample for different pressures.

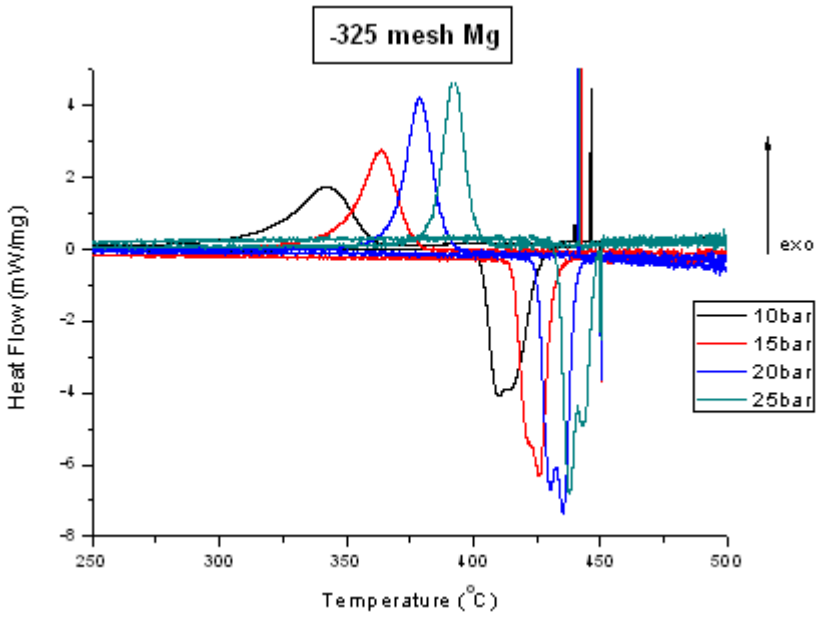

Fig. 4.18: DSC results of the Mg -325 mesh powdered sample under 10, 15, 20 and 25 bar H_2 pressure (5°C/min heating rate).

An endothermic peak in the reaction which is attributed to hydrogen desorption and an exothermic peak corresponding to the absorption and formation of MgH_2 are observed in the DSC results above. As 3 bar hydrogen pressure was below the plateau pressure for MgH_2, no absorption was observed at this pressure value. Similar patterns resulted from the rest of the Mg samples apart from the nanopowders (Metal Nanopowders Ltd.) (3.197mg) which under a 25 bar pressure of H_2 did not show either absorption or desorption peaks. This might be due to oxidation of the sample during the fabrication process and/or during the transfer process (under Ar) to the DSC. Unfortunately the sample size for the nano-Mg powder was too small to allow a conventional powder x-ray diffraction measurement to be carried out which would verify oxidation of the sample. Capillary XRD, FT-IR, SEM-EDS and/or Raman Spectroscopy may be used to measure the Mg oxide/hydroxide present in the Mg samples. The DSC results for the 500 mesh Mg and the MgH2 powder samples are presented in figures 4.19(a) and 4.19(b) respectively.

(a) **DSC results for 500 mesh Mg powder**

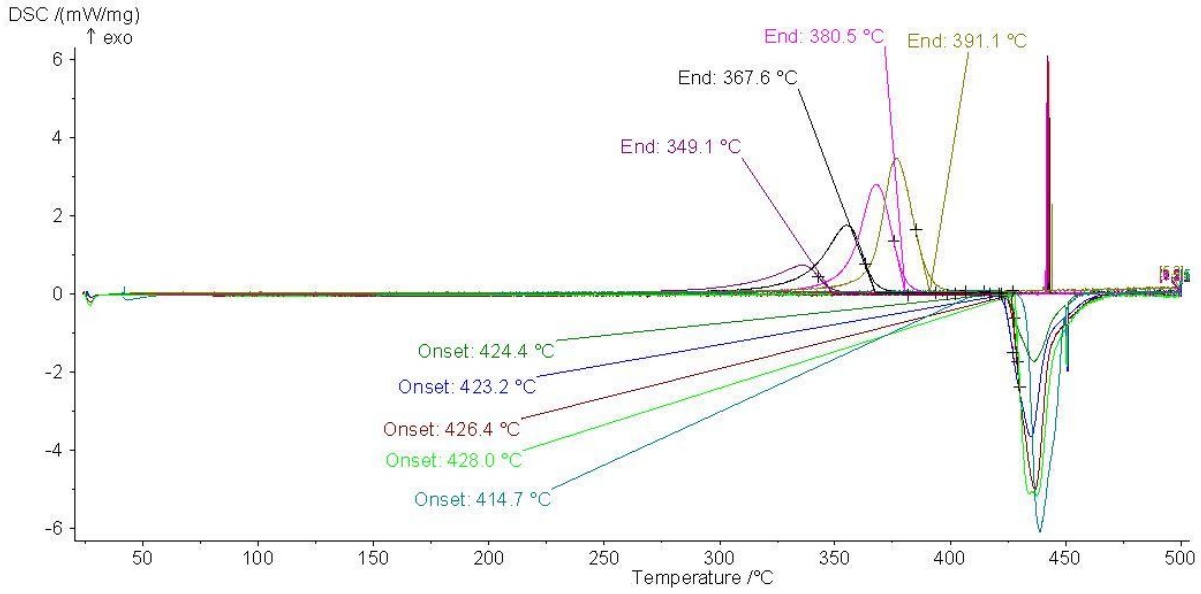

(b) **DSC results for MgH_2 powder**

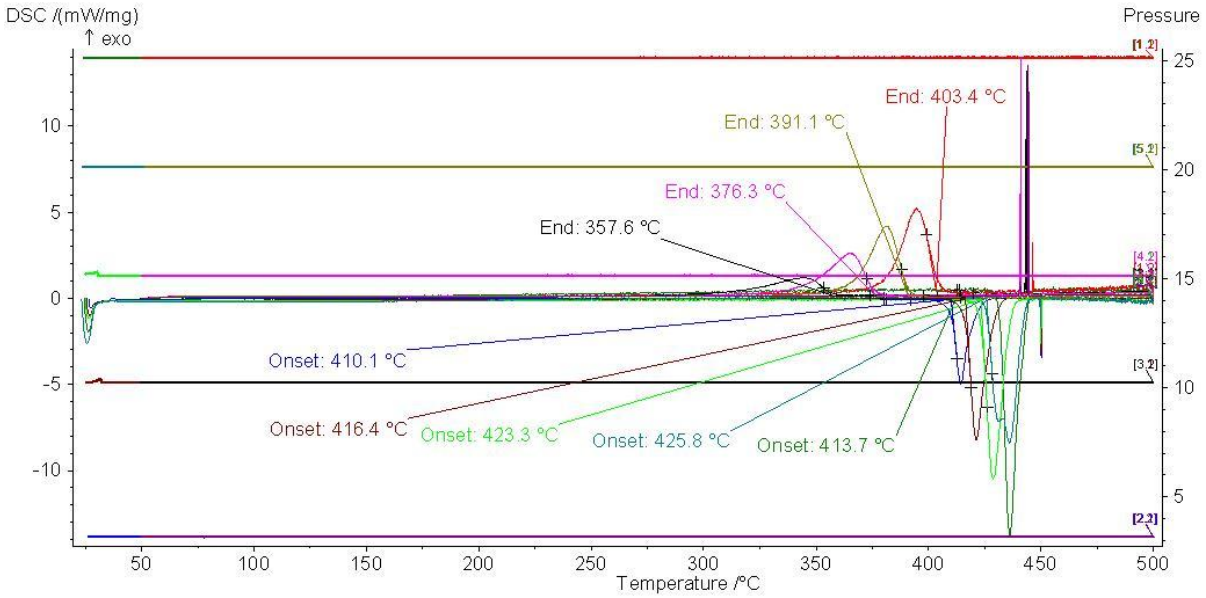

Fig. 4.19: DSC results of the (a) Mg 500 mesh and (b) MgH_2 powder samples under 10, 15, 20 and 25 bar H_2 pressure (5°C/min heating rate).

From the overall results of all the Mg powders we were able to determine the onset temperatures of hydrogen absorption and desorption which correspond to the different pressures of H_2. The values of these temperatures were determined with the use of the Netzsch Proteus software by taking the intersection between the background line and the slope of the peak and are presented in Table 4.2.

Table 4.2: Onset temperatures of hydrogen absorption/desorption for -325 mesh Mg, 500 mesh Mg and MgH2 powders under 3, 10, 15, 20 and 25 bar hydrogen gas (5°C/min heating rate).

H_2 Pressure (bar)	**-325 mesh Mg powder**		**500 mesh Mg powder**		**MgH_2 powder**	
	Absorption temp.(°C)	*Desorption temp.(°C)*	*Absorption temp.(°C)*	*Desorption temp.(°C)*	*Absorption temp.(°C)*	*Desorption temp.(°C)*
3	-	395.1	-	424.4	-	410.1
10	359.7	403.1	349.1	423.2	357.6	416.4
15	375.4	415.9	367.6	426.4	376.3	423.3
20	389.1	424.9	380.5	428.0	391.1	425.8
25	400.5	433.0	391.1	414.7	403.4	413.7

These allow the estimation of the enthalpy ΔH, which derives once again from the formation of the van't Hoff plots (lnP versus 1/T). The onset temperatures of both absorption and desorption display an increase when the hydrogen pressure increased throughout the DSC measurements for all the powder samples. The van't Hoff plots and the error analysis of hydrogen absorption and desorption of the -325 mesh Mg powder, the 500 mesh Mg and MgH_2 powders are shown in figure 4.20(a) and 4.20(b) and 4.20(c) respectively. The error for the DSC was +/- 0.5°C and +/- 0.3 bar. These values gave rise to significantly small error bars thus proving accuracy of our results. From these plots, the enthalpies of absorption and desorption were calculated for each sample. For the sample from Alpha Aesar of -325 mesh particle size the enthalpies of absorption and desorption were found to be -79.4 kJ/mol and -122.25 kJ/mol respectively. The 500 mesh sample from Magnesium Elektron exhibited a -75 kJ/mol enthalpy of absorption of while that of the magnesium hydride sample from

Goldschmidt showed an absorption enthalpy about -71 kJ/mol. The sample with the smallest particle size (500 mesh) displays a smaller enthalpy of absorption compared to that of the 325 mesh sample.

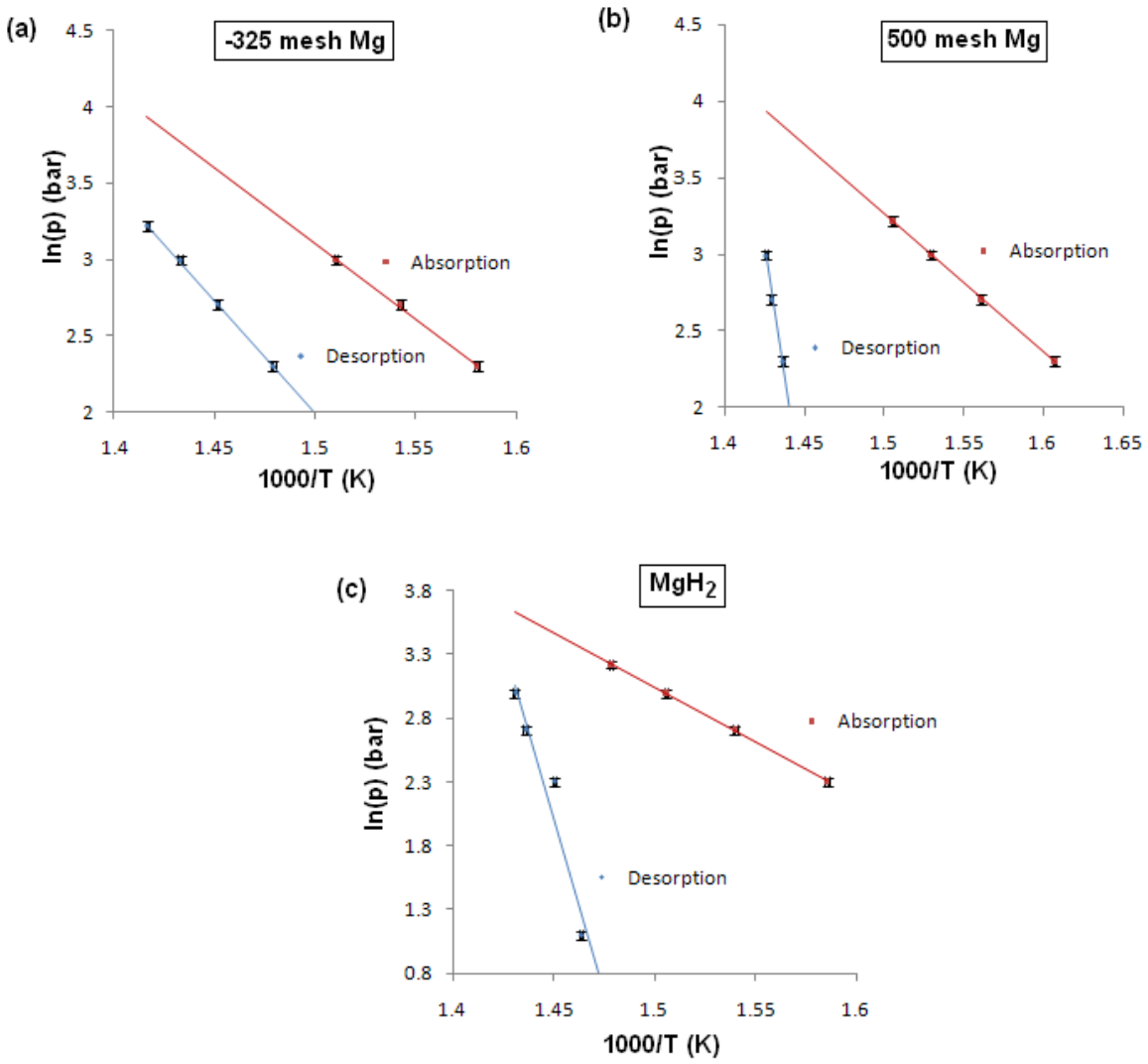

Fig. 4.20: Van't Hoff plots and error bars of absorption and desorption of the (a) -325 mesh Mg, (b) 500 mesh Mg and (c) MgH_2 powders.

This result is in agreement with Varin et al. who suggest a relationship between the particle size and the type of hydride phase present and hence the enthalpies of absorption/desorption [22]. Moreover, the absorption enthalpy of the MgH_2 sample was lower than the previous two samples. XRD studies on these Mg/MgH_2 powders would allow us to investigate which

hydride phases are present, their relative proportions and to estimate the grain sizes. The desorption enthalpy of the -325 mesh sample was found to be quite high (-122.25 kJ/mol) compared to the average value of formation and decomposition of MgH_2 which is -75 kJ/mol. For the 500 mesh and MgH_2 samples the determination of the desorption enthalpies was very difficult due to the very high deviations of certain points in the van't Hoff plots (data points were very scattered). Even after removing the problematic points of these plots (corrected desorption van't hoff plots are shown in figure 4.20) the slopes and therefore the enthalpies of desorption were found to be extremely high (>300 kJ/mol).

4.3 Conclusions

In this work the structural and hydrogenation properties of pure nano-magnesium in the form of variable particle size powders as well as a thin film were investigated. Moreover, we studied the hydrogen storage performance of Mg/Ti thin film multilayer structures with respect to the number of deposited layers of both materials, while preserving the total amount of Mg within the structure.

Pure Mg films as well as Mg/Ti thin film structures were successfully deposited upon various substrate types using a magnetron sputtering system while the amount of Mg in all sample types was kept constant. Using SEM we were able to observe the structures of the film samples while no clear signs of oxidation of these samples were visible. EDS measurements on the samples showed the existence of Mg and Ti while the presence of oxygen was limited to < 2 atomic%. On the other hand, EDS was ineffective in showing a distinct alternation in the composition of the layers as the Ti layers were very thin when compared to the spot size of the beam, as well as the existence of an 'intermixed' zone (co-

sputtered zone of Mg and Ti) between the layers causing difficulty during the selection of the points of the line spectrum.

XRD results prior to hydrogenation on the Mg as well Mg/Ti films showed that all samples were preferentially orientated along the (002) crystal plane while the Mg powder displayed its greatest peak at the (101) plane. These results are in agreement with previous studies which have shown preferential growth of Mg films along the c-axis [26-28]. Differences in the sputtering conditions of the Mg/Ti samples gave rise to differences in their XRD patterns. Furthermore, the XRD results also showed evidence of intrinsic stresses within the films and the possible presence of 'intermixed' zones at the interfaces of the multilayered samples.

Using a Sieverts (Hiden HTP) apparatus the thin film samples were hydrided. This was confirmed after removing one slide of each sample from the HTP and carrying out XRD measurements. From the remaining slides, PCI diagrams were obtained using the HTP, which allowed van't Hoff plots and the desorption enthalpies of each sample to be calculated. The desorption enthalpies were found to be quite high compared to the literature. While the large errors of the van't Hoff plots due not render these results reliable.

TPD measurements displayed similar temperatures of hydrogen desorption for all three thin film samples. The 40 layered sample appeared not to have completely desorbed, which was later confirmed using XRD, while the appearance of bubbles on the sample surface might indicate the detachment of layers within the film causing less influence of the cooperative phenomena. The TPD results on the pure Mg and 20 layered Mg/Ti film displayed a two step desorption process most likely due to the existence of a metastable γ-MgH_2 phase. This was

not confirmed during the final XRD measurements as the peaks obtained were very weak due to the Kapton tape.

Kinetic points using the HTP showed the fastest kinetics during hydrogen absorption for the 40 layered structure. However, in the case of hydrogen desorption the 20 layered sample exhibited the fastest kinetics of all three samples.

IGA measurements on the Mg sample showed no hydrogen uptake proving this method difficult for measuring hydrogen storage properties of Mg films due to the lack of sensitivity of the IGA balance, in this particular configuration.

Finally, DSC experiments on Mg powders of different particle sizes as well as on the MgH_2 sample as a function of hydrogen pressure showed an onset temperature (of both absorption and desorption) peak shift towards higher values when the hydrogen pressure increased in agreement with van't Hoff's equation (paragraph 1.3.2). The results also showed the lowest enthalpy of absorption for the MgH_2 sample. Moreover, when comparing the Mg powders the sample with the smallest particle size displayed the lowest absorption enthalpy. This result is in agreement with Varin et al who suggest a correlation between particle size and the present hydrided phases of Mg, thus affecting the thermodynamics of Mg [22]. All desorption enthalpies of the samples were found to be quite high. Due to oxidation issues the nano-Mg powder showed no signs of absorption or desorption. Reducing the grain size of the material constitutes another promising approach to improve the performance of Mg powders by enhancing hydrogen diffusion along the grain boundaries rather than through the metal

lattice [16]. Additionally, grain boundaries act as favourable nucleation sites for the formation and decomposition of the hydride phase.

4.4 Future Work

Future work should focus on the production and investigation of various types of Mg/Ti thin film multilayer structures. A better monitoring of the hydrogen storage properties with respect to the structure of the samples may be achieved through the manufacturing of more Mg/Ti samples with a variety of numbers of layers. Varying the thickness of the Mg and/or Ti layers and the induced influence on the sorption properties may be investigated. Furthermore, the creation of Mg/Ti films with areas of coexistence of both materials as well as the degree of their coexistence may also constitute an area of study. Another variable that would be of certain interest is the type of substrate used for the thin film samples either using different types of material or using a substrate with or without a particular crystallographic orientation.

Apart from the above the use of different techniques for the determination of the sorption properties of the Mg/Ti samples may be investigated. For example, resistivity measurements may also be carried out on thin films deposited on glass substrates (metal substrates are conductive and may also absorb hydrogen). The introduction of hydrogen in a material causes change in the electrical resistivity as the hydride being formed is an insulator therefore the onset temperatures of absorption/desorption can be determined. In situ XRD measurements at different pressures could be used to investigate the induced stresses within Mg/Ti multilayer samples. XRD measurements may also be used to confirm the presence of the γ-phase MgH_2 within the samples.

Finally, in the case of magnesium powders in order to avoid oxidation and difficulties which arise while handling samples in the form of a solution, magnesium nanopowders may be provided in a dry state. Furthermore nano-particles of Ti can be distributed on the nano-Mg surface and the hydrogen storage characteristics of these materials can be investigated and compared with the results on the Mg nanopowders. Apart from using the DSC to determine the onset sorption temperatures, the powdered samples can also be measured on the IGA or on a HTP system in order to measure the hydrogen uptake and sorption kinetics. Furthermore, XRD studies may be used to investigate the present hydride phases (their relative proportions) and estimate the grain sizes of Mg/MgH_2 powders.

References

[1] G. W. Crabtree, M. S. Dresselhaus and M. V. Buchanan; The hydrogen economy. Physics Today (2004) 39-44

[2] E. MacA. Gray; Hydrogen storage – status and prospects. Advances in Applied Ceramics 106 (2007) 25-28

[3] A. Züttel; Materials for hydrogen storage. Materials Today (2003) 24-33

[4] D.K. Ross; Hydrogen storage: The major technological barrier to the development of hydrogen fuel cell cars. Vacuum 80 (2006) 1084–1089

[5] M. Dornheim, S. Doppiu, G. Barkhordarian, U. Boesenberg, T. Klassen, O. Gutfleisch and R. Bormann. Scripta Materialia 56 (2007) 841–846

[6] B. Sakintuna, F. Lamari-Darkrim and M. Hirscher; Metal hydride materials for solid hydrogen storage:Areview. International Journal of Hydrogen Energy 32 (2007) 1121 – 1140

[7] US Department of Energy, Office of Basic Energy Sciences, Basic Research Needs for the Hydrogen Economy, US DOE, Washington, DC, (2004)

[8] David Book; Lectures on hydrogen storage and fuel cells (2008)

[9] K. Young, T. Ouchi, M.A. Fetcenko, Pressure-Composition-Temperature Hysteresis in C14 Laves Phase Alloys: Part 1 Simple Ternary Alloys, Journal of Alloys and Compounds (2008)

[10] S. N. Klyamkin, M. T. Hagström, E. V. Mescheryakova and P. D. Lund; Hysteresis in Ce-based AB_5-type metal hydrides. Journal of Material Science 35 (2000) 133-137

[11] A. Y. Esayed and D. O. Northwood; Hysteresis in metallic solid solution and intermetallic compound-hydrogen systems. International Journal of Hydrogen Energy 22 (1997) 77-82

[12] M. Bououdina, D. Grant and G.Walker; Review on hydrogen absorbing materials—structure, microstructure, and thermodynamic properties. International Journal of Hydrogen Energy 31 (2006) 177 – 182

[13] E. David; An overview of advanced materials for hydrogen storage. Journal of Materials Processing Technology 162–163 (2005) 169–177

[14] Vincent Bérubé, G. Radtke, Mildred Dresselhaus and Gang Chen; Size effects on the hydrogen storage properties of nanostructured metal hydrides: A review. International Journal of Energy Research 31 (2007) 637–663

[15] O. Friedrichs, J.C. Sánchez-López, C. López-Cartes, M. Dornheim, T. Klassen, R. Bormann and A. Fernández; Chemical and microstructural study of the oxygen passivation behaviour of nanocrystalline Mg and MgH_2. Applied Surface Science 252 (2006) 2334–2345

[16] A. Zaluska, L. Zaluski and J.O. Ström–Olsen; Nanocrystalline magnesium for hydrogen storage. Journal of Alloys and Compounds 288 (1999) 217–225

[17] H. Imamura, K. Masanari, M. Kusuhara, H. Katsumoto, T. Sumi and Y. Sakata; High hydrogen storage capacity of nanosized magnesium synthesized by high energy ball-milling. Journal of Alloys and Compounds 386 (2005) 211–216

[18] N. Hanada, T. Ichikawa, S. I. Orimo and H. Fujii; Correlation between hydrogen storage properties and structural characteristics in mechanically milled magnesium hydride MgH_2. Journal of Alloys and Compounds 366 (2004) 269–273

[19] A. Walton, K. Ruzalla, M. Al-Mamouri, V.S.J. Mann, D. Book, J.D Speight, I.R. Harris, J. Pendergast, S. Johnson and P.A. Anderson, MH2004, Krakow, Poland, September 2004.

[20] J. Huot , G. Liang, S. Boilya, A. Van Neste and R. Schulz; Structural study and hydrogen sorption kinetics of ball-milled magnesium hydride. Journal of Alloys and Compounds 293–295 (1999) 495–500

[21] F.C. Gennari, F.J. Castro and G. Urretavizcaya; Hydrogen desorption behaviour from magnesium hydrides synthesized by reactive mechanical alloying. Journal of Alloys and Compounds 321 (2001) 46–53

[22] R A Varin, T Czujko and Z Wronski; Particle size, grain size and γ -MgH_2 effects on the desorption properties of nanocrystalline commercial magnesium hydride processed by controlled mechanical milling. Nanotechnology 17 (2006) 3856–3865

[23] Y. Zhang, S. Liao, Y. Fan, J. Xu and F. Wang; Chemical reactivities of magnesium nanopowders. Journal of Nanoparticle Research 3 (2001) 23–26

[24] K. F. Aguey-Zinsou and J. R. Ares-Fernández; Synthesis of colloidal magnesium: a near room temperature store for hydrogen. Chemistry of Materials 20 (2008) 376–378

[25] S. Singh, S.W.H. Eijt, M.W. Zandbergen, W.J. Legerstee and V.L. Svetchnikov; Nanoscale structure and the hydrogenation of Pd-capped magnesium thin films prepared by plasma sputter and pulsed laser deposition. Journal of Alloys and Compounds 441 (2007) 344–351

[26] A. Léon, E.J. Knystautas, J. Huot and R. Schulz; Hydrogenation characteristics of air-exposed magnesium films. Journal of Alloys and Compounds 345 (2002) 158–166

[27] L. Pranevicius, D. Milcius, L.L. Pranevicius, C. Templier, B. Bobrovaite and I. Barnackas; The role of grain boundaries in the mechanism of plasma immersion hydrogenation of nanocrystalline magnesium films. Applied Surface Science 252 (2006) 4202–4208

[28] L. Pranevicius, D. Milcius, L.L. Pranevicius and G. Thomas; Plasma hydrogenation of Al, Mg and MgAl films under high-flux ion irradiation at elevated temperature. Journal of Alloys and Compounds 373 (2004) 9–15

[29] C.W. Ostenfeld, M. Johansson and I. Chorkendorff; Hydrogenation properties of catalyzed and non-catalyzed magnesium films. Surface Science 601 (2007) 1862–1869

[30] W. Oelerich, T. Klassen and R. Bormann; Metal oxides as catalysts for improved hydrogen sorption in nanocrystalline Mg-based materials. Journal of Alloys and Compounds 315 (2001) 237–242

[31] P. Hjort, A. Krozer and B. Kasemo; Hydrogen sorption kinetics in partly oxidized Mg films. Journal Of Alloys and Compounds 237 (1996) 74-80

[32] Y. Song, Z.X. Guo and R. Yang; Influence of titanium on the hydrogen storage characteristics of magnesium hydride: a first principles investigation. Materials Science and Engineering A 365 (2004) 73–79

[33] X. Xu and C. Song; Improving hydrogen storage/release properties of magnesium with nano-sized metal catalysts as measured by tapered element oscillating microbalance. Applied Catalysis A: General 300 (2006) 130–138

[34] P. Wang, A.M. Wang, H.F. Zhang, B.Z. Ding and Z.Q Hu; Hydrogenation characteristics of Mg–TiO_2 (rutile) composite. Journal of Alloys and Compounds 313 (2000) 218–223

[35] M. Tsuda, W. A. Dino, H. Kasai, H. Nakanishi and H. Aikawa; Mg–H dissociation of magnesium hydride MgH_2 catalyzed by 3d transition metals. Thin Solid Films 509 (2006) 157 – 159

[36] G. Liang, J. Huot, S. Boily, A. Van Neste and R. Schulz; Catalytic effect of transition metals on hydrogen sorption in nanocrystalline ball milled MgH –Tm (Tm5Ti, V, Mn, Fe and Ni) systems. Journal of Alloys and Compounds 292 (1999) 247–252

[37] N. Hanada, T. Ichikawa and H. Fujii; Catalytic effect of nanoparticle 3d-Transition metals on hydrogen storage properties in magnesium hydride MgH_2 prepared by mechanical milling. Journal of Physical Chemistry B 109 (2005) 7188-7194

[38] J. L. Bobet, C. Even, Y. Nakamura, E. Akiba and B. Darriet; Synthesis of magnesium and titanium hydride via reactive mechanical alloying. Influence of 3d-metal addition on MgH_2 synthesize. Journal of Alloys and Compounds 298 (2000) 279–284

[39] M. Abdellaoui, D. Cracco and A. Percheron-Guegan; Structural investigation and solid-H_2 reaction of Mg_2Ni rich nanocomposite materials elaborated by mechanical alloying. Journal of Alloys and Compounds 293–295 (1999) 501–507

[40] Y. Song, Z. X. Guo and R. Yang; Influence of selected alloying elements on the stability of magnesium dihydride for hydrogen storage applications: a first principles investigation. Physical review B 69 (2004) 094205

[41] G. Liang and R. Schulz; Synthesis of Mg-Ti alloy by mechanical alloying. Journal of Materials Science 38 (2003) 1179-1184

[42] D. Kyoi, T. Sato, E. Rönnebro, N. Kitamura, A. Ueda, M. Ito, S. Katsuyama, S. Hara, D. Noréus and T. Sakai; A new ternary magnesium–titanium hydride Mg_7TiH_x with hydrogen desorption properties better than both binary magnesium and titanium hydrides. Journal of Alloys and Compounds 372 (2004) 213–217

[43] P. Vermeulen, R.A.H. Niessen and P.H.L. Notten; Hydrogen storage in metastable $Mg_yTi_{(1-y)}$ thin films. Electrochemistry communications 8 (2006) 27-32

[44] P. Vermeulen, H. J. Wondergem, P. C. J. Graat, D. M. Borsa, H. Schreuders, B. Dam, R. Griessen and P. H. L. Notten; In situ electrochemical XRD study of (de)hydrogenation of Mg_yTi_{100-y} thin films. Journal of Materials Chemistry 18 (2008) 3680-3687

[45] H. Fujii, K. Higuchi, K. Yamamoto , H. Kajioka , S. Orimo and K. Toiyama; Remarkable hydrogen storage, structural and optical properties in multi-layered Pd/Mg thin films. Materials Transactions 43 (2002) 2721-2727

[46] K. Higuchi, K. Yamamoto, H. Kajioka, K. Toiyama, M. Honda, S. Orimo and H. Fujii; Remarkable hydrogen storage properties in three-layered Pd/Mg/Pd thin films. Journal of Alloys and Compounds 330–332 (2002) 526–530

[47] K. Yoshimura, Y. Yamada and M. Okada; Hydrogenation of Pd capped Mg thin films at room temperature. Surface Science 566-568 (2004) 751-754

[48] K. Higuchi, H. Kajioka, K. Toiyama, H. Fujii, S. Orimo and Y. Kikuchi; In situ study of hydriding-dehydriding properties in some Pd/Mg thin films with different degree of Mg crystallization. Journal of alloys and compounds 293-295 (1999) 484-489

[49] S. YE, L. Ouyang and M. Zhu; Hydrogen storage properties of preferentially orientated Mg-Ni multilayer prepared by magnetron sputtering. Rare Metals 25 (2006) 295

[50] R. Domènech-Ferrer, Madana Gurusamy Sridharan, G. Garcia, F. Pi, J. Rodriguez-Viejo; Hydrogenation properties of pure magnesium and magnesium–aluminium thin films. Journal of Power Sources 169 (2007) 117–122

[51] A. Krozer and B. Kasemo; Unusual kinetics due to the interface hydride formation in the hydriding of Pd/Mg sandwitch layers. Journal of Vacuum Science and Technology A 5 (1987) 4

[52] A. Fischer, H. Köstler and L. Schlapbach; Hydrogen in magnesium alloys and magnesium interfaces: preparation, electronic properties and interdiffusion. Journal of the Less Common Metals 172-174 (1991) 808-815

[53] J. Paillier, S. Bouhtiyya, G.G. Ross and L. Roué; Influence of the deposition atmosphere on the characteristics of Pd–Mg thin films prepared by pulsed laser deposition. Thin Solid Films 500 (2006) 117 – 123